FACULTY OF SCIENCE
UNIVERSITY OF COPENHAGEN

Master's thesis

Mergers produce outliers from the fundamental metallicity relation

Asger Emil Grønnow
agronnow@dark-cosmology.dk

Supervisors:
Kristian Finlator
Lise Christensen

DARK Cosmology Centre
Niels Bohr Institute
University of Copenhagen
December 1, 2014

Abstract

During a merger between spiral galaxies, the primary galaxy undergoes a period of strong infall of gas towards the center. As the disks typically have metallicity gradients with the metallicity decreasing exponentially with radius, this infall dilutes the central gas metallicity. So far this effect has been studied through samples of galaxy pairs and simulations of merging galaxies. In this thesis I examine the effect mergers have on metallicity in a new way based on the asymmetry of the scatter of the Fundamental Metallicity Relation (FMR), which relates the gas metallicity, stellar mass and star formation rate of galaxies. Selecting a sample of $\sim 170,000$ galaxies at $z \sim 0.1$ from the Sloan Digital Sky Survey (SDSS), I fit an FMR and compute the residual metallicities. I find an overabundance of galaxies with lower than expected metallicities as was also noted in Mannucci et al. (2010). The galaxies in this tail form a physically distinct population with lower stellar masses, enhanced star formation rates and smaller half-light radii than the rest of the sample, consistent with them being merging galaxies. The existence of the tail is robust to the choice of metallicity calibration. I develop a simple model for the distribution of metallicity residuals, where mergers dilute metallicity by an amount proportional to the mass ratio of the merger. This model provides an excellent fit to the data using three free parameters pertaining to the magnitude and time-scale of the dilution and a lower mass ratio threshold. The metallicity depressions and time-scales I find are in good agreement with estimates from hydrodynamical merger simulations and observational studies of close galaxy pairs. These findings support the suggestion by (Mannucci et al., 2010) that mergers leave a signature in the FMR.

Acknowledgements

I would like to thank my supervisors Kristian Finlator and Lise Christensen for the time and energy that they dedicated to guide me throughout the 15 months of this project. They have both taken the role as master's supervisor very seriously and have shown consistent interest in the project. I also thank Filippo Mannucci and Sara Ellison for helpful discussions during their visits at Dark Cosmology Centre.

Contents

1 Outline

This thesis basically consists of two parts. The appendix contains an article, which has been submitted to Monthly Notices of the Royal Astronomical Society, wherein the data, the model and the results are described and discussed. The purpose of the text outside the appendix is to introduce the concepts underlying the model in much more detail than the short introduction in the article does, as well as provide a more detailed conclusion. It also includes a short summary of the project described in the article, in a less technical language. Therefore the reading order should be *Metallicity*, *Galaxy mergers* and *The mass-metallicity relation and second-parameter dependencies* followed by the article in the appendix, followed by *Conclusions and future work*.

2 Metallicity

In astronomy and astrophysics all elements heavier than helium (i.e. not hydrogen and helium) are called "metals". The metallicity is the fraction of mass that is in the form of metals; this can either be locally in a single star or part of the interstellar medium (ISM) or globally as an average over all stars or the entire ISM in a galaxy. In this thesis, we always mean the metallicity of the ISM of a galaxy unless otherwise stated.

The simplest measure of metallicity is $Z \equiv M(\mathrm{He}<)/M$, where $M(\mathrm{He}<)$ is the total mass of all gas heavier than helium and M is the mass of all gas (this is, of course, the same as the ratio of the densities, N). Some relatively simple analytical models of the metallicity evolution in galaxies, which are summarised in Tinsley (1980), were developed in the 1960s and 1970s. The simplest of these is the closed-box model which assumes that there are no flows of gas leading material in or out of the galaxy, such that the total baryonic mass stays constant, and that the ISM is well-mixed, such that the metallicity is independent of position. If we assume that stars return a fraction R of their mass to the ISM immediately after being formed, that the initial metallicity was zero and a time-independent initial mass function (IMF), we get that the metallicity is simply proportional to the logarithm of the ratio between the initial gas mass and the current gas mass so long as $Z \ll 1$. The constant of proportionality is called the "effective yield" and depends on R and how efficient stars are at producing metals from hydrogen and helium (the "yield"). Obviously, in such a model the metallicity can never decrease and if we further assume that the star formation rate (SFR) is proportional to the gas mass, the metallicity will simply be proportional to the time elapsed since $Z = 0$.

The closed-box model has the serious flaw of predicting a significantly too high fraction of metal-poor stars compared to what is observed (this is called the "G-dwarf problem"). This problem can be alleviated by relaxing the assumption of a closed system. The simplest way of doing this is to add an inflow of pristine ($Z = 0$) gas that exactly balances the gas lost to star formation (Larson, 1972), but a more general model with both inflow and outflow and a non-constant gas mass will also solve the G-dwarf problem. In such models the metallicity typically tends asymptotically towards the yield.

2.1 Addition of metals to the ISM

Initially the ISM was nearly pristine, as big bang nucleosynthesis produced 75 per cent ^{1}H, 25 per cent ^{4}He and only trace amounts of slightly heavier nuclei such as deuterium and lithium (Coc et al., 2004). This is due to Helium-4 being very tightly bound for its mass, and the fact that there are no stable nuclei with atomic number $A = 5$. Aside from a few of the lighter elements such as boron, which can be produced by cosmic rays interacting with the ISM, metals are produced only in stars in a process called stellar nucleosynthesis.

The majority of a star's lifetime is spent in the main sequence phase, where hydrogen nuclei fuse to produce helium in the core. The net reaction is $4\,^1\mathrm{H} \rightarrow\ ^4\mathrm{He} + 2\mathrm{e}^+ + 2\nu_e$ which can occur in four different ways. The three so-called PP chains proceed through deuterium, lithium, beryllium and boron while the "CNO cycle" proceed through carbon, nitrogen and oxygen (hence the "CNO") with carbon acting as a catalyst. The rate of these reactions strongly depend on temperature, and therefore the mass of the star, with dwarfs producing all their helium through the PP chains and the CNO cycle completely dominating in moderate and high-mass stars (Stahler

& Palla, 2005). When hydrogen becomes sparse in the core, the decreased reaction rate diminishes the pressure support of the core and the core contracts causing the temperature to increase. The core eventually becomes hot enough for helium to fuse to carbon. This process of the core fusing elements until one of them is mostly depleted, after which the core loses support and contracts until another fusion reaction sets in, continues up to oxygen burning which produces elements up to magnesium. Many elements are also created by photodissociation, i.e. nuclei being broken up by high-energy gamma ray photons. Heavier elements up to nickel are created through a complex network of reactions driven mainly by capture of helium nuclei (α-capture), where a heavier nucleus and a photon are produced, e.g. $S^{32}+{}^4\text{He} \rightarrow {}^{36}\text{Ar}+\gamma$. α-capture releases energy only for elements up to nickel, after which it requires energy. Therefore, heavier elements are instead produced through neutron capture(s) followed by beta decay, i.e. $(Z, A) + n \rightarrow (Z, A + 1) + \gamma$ followed by $(Z, A + 1) \rightarrow (Z + 1, A + 1)+\text{e}^- + \overline{\nu}_e$. This process can produce heavy nuclei that cannot be produced by fusion reactions because there is no Coulomb barrier to overcome in neutron capture. Some elements require very high neutron fluxes to be synthesized because the required chain of neutron captures goes through unstable nuclei with short half-lives. These are called r-process elements and cannot be produced through regular stellar nucleosynthesis. Possible sites of the r-process are the region just above a proto-neutron star during a core-collapse supernova, highly asymmetric supernovae with jets or merging neutron stars (Woosley et al., 2002; Ramirez-Ruiz et al., 2014). The other type of neutron capture elements, s-process elements, which are produced through neutron captures of nuclei with long half-lives, are believed to be synthesized by late-stage giant stars that can produce moderate neutron fluxes through reactions such as ${}^{13}\text{C}+{}^4\text{He} \rightarrow {}^{16}\text{O}+n$ (Busso et al., 1999).

Some of the elements produced in stars are ejected into the ISM through supernovae (SNe) and winds. Stars of all masses eject a significant fraction of their mass in a "superwind" shortly before becoming a white dwarf or exploding in a supernova (Willson, 2000; Smith, 2014). During this phase they occupy a part of the colour-magnitude diagram known as the "Asymptotic Giant Branch" (AGB). As this ejecta originates from the outer parts of stars, it is mostly unprocessed matter which therefore has the same metallicity as the gas the star initially formed from. However, at the onset of the AGB phase a star undergoes a process called "third dredge-up" that transports matter from the deeper layers to the surface, where it can be expelled in the wind. This is unimportant for metallicity in general, but a significant amount of carbon is expelled in this way (Oppenheimer & Davé, 2008).

Stars with masses less than $\sim 1M_\odot$ have such long main sequence life times that they for many purposes effectively lock up their material permanently, though. Stars of masses $\gtrsim 8M_\odot$ end up exploding in core-collapse supernovae after at most $\sim 10^8$ years, leaving a neutron star or a black hole remnant. The fraction of their mass that they eject depends on the mass. Stars with masses in the range $\sim 8 - 40M_\odot$ leave a remnant containing 10–40 per cent of the mass. Stars with masses in the range $\sim 40 - 140M_\odot$ might not explode at all but leave all the mass in the black hole remnant (Fryer, 1999), while extremely massive stars with $M > 140M_\odot$ explode in pair instability SNe which leaves no remnant at all (Ryan & Norton, 2010). Some elements, such as iron group elements, are predominantly produced in type Ia SNe rather than core-collapse SNe. This is an important distinction as type Ia SNe occur on a much longer time-scale than core-collapse SNe.

Galaxies can also theoretically increase their metallicity by accreting enriched gas from the intergalactic medium (IGM). While not pristine, infalling IGM gas tends to be metal-poor (Giavalisco et al., 2011; Bouché et al., 2013) so it will typically dilute, rather than enrich, the ISM of a galaxy. Nonetheless, satellite galaxies in high-density regions accreting gas enriched by outflows from massive galaxies might partially explain why satellite galaxies tend to have high metallicities for their masses (Davé et al., 2011).

2.2 Measuring metallicity

Metallicity is not measured according to the definition $Z \equiv N(\text{He}<)/N$, but rather with a single heavy element as a substitute for all metals and hydrogen as a substitute for all gas. Stellar metallicities are usually measured as [Fe/H] which is the logarithm of the ratio of the total mass or density of iron to hydrogen, relative to the Sun. For gas metallicities the standard measure is $12 + \log(\text{O/H})$, i.e. the logarithm of the ratio of oxygen to hydrogen with a constant term added for historical reasons. This is the most common measure primarily because oxygen

produces the strongest emission lines. In addition, oxygen is well-suited as a proxy of the general metallicity as it is an α-process element that is spread by short-lived stars, so that it tracks the metallicity essentially instantly. In contrast, elements such as iron are associated with type Ia supernovae and are therefore delayed relative to the more common α-process elements on Gyr time-scales, making them poor representatives of the overall metallicity in the ISM. Oxygen comprises about 50 per cent of all metals in the Universe (López-Sánchez et al., 2012).

For Damped Lyman-α (DLA) systems, which are found at high redshifts and are observed as absorption along the line-of-sight of quasars, the gas metallicity can be inferred from absorption lines, typically those of Zinc (Wolfe et al., 2005). For galaxies though, gas phase metallicities are estimated from the relative intensities of two or more emission lines. The methods are divided into two types: *direct methods* and *strong-line methods*.

2.2.1 Direct method

In the direct method the metallicity is inferred from the electron temperature and density of HII regions. Metals are efficient coolants, so gas-phase metallicity is anti-correlated with gas temperature. The temperature is found from the ratio of the intensities of two emission lines that are emitted from the same ion but at two widely separated excitation energies. As it is the same ion the densities cancel out in the ratio, so the difference in intensities depends only on how rare the highly excited ions are relative to the less excited ions, which depends strongly on temperature. Popular choices are OIII and NII as these have ions with considerably different excitation energies that both emit in optical wavelengths (Osterbrock & Ferland, 2006). Conversely, the density is found from the ratio of the intensities of two emission lines that are emitted from the same ion at *almost similar* excitation energies. In this case, the intensity ratio is a measure of the relative collisional strengths at nearly equal temperatures which depends on the electron density.

The main problem with the direct method is that highly excited lines are weak, so that very high signal-to-noise spectra are required. Thus, it is not possible in most cases to find the metallicities of single galaxies using the direct method. For a large sample of galaxies such as the SDSS average metallicities can be found by stacking spectra (the stacking causes some of random noise to cancel out thus raising signal-to-noise). For instance, Andrews & Martini (2013) found a mass-metallicity relation for a large SDSS sample (see §4) using the direct method by binning galaxies by mass and stacking the spectra for the galaxies in each bin. Stacking spectra, however, removes any knowledge of the scatter in the inferred metallicities. Another problem with the direct method is that metallicities inferred from collisionally excited lines differ significantly from metallicities inferred from recombination lines. The source of this discrepancy is currently unknown (Osterbrock & Ferland, 2006), but may be due to temperature fluctuations within the measured HII regions causing metallicities derived from collisionally excited lines to be underestimated (López-Sánchez et al., 2012).

2.2.2 Strong-line methods

In order to obtain metallicity measurements of HII regions and galaxies without the often prohibitively high signal-to-noise required for the direct method, strong-line methods were developed. These methods use ratios of strong emission lines only. There are two types of strong-line methods: Empirical and theoretical.

Empirical methods are based on HII regions that have had their metallicities measured by the direct method in addition to the strong lines of choice. For suitable combinations of strong lines, there should be a correlation with metallicity as measured from electron temperature though the scatter will be quite large. Obviously, the accuracy of such a calibration depends on the accuracy of the direct method used, and so the derived strong-line method becomes subject to the same caveats as the direct method. The range of validity of the calibration is also limited by the sample of HII regions used.

Theoretical methods are based on photoionization models. Thus they do not depend on other methods and can be extended to a wide range of metallicities. They also naturally yield the strong-line intensity dependence on the ionization parameter (see further below). They are, however, limited by the accuracy of the photoionization model used. These models might not be very accurate as they have to assume spherical or plane-parallel geometries and a homogeneous distribution of gas and dust (Kewley & Ellison, 2008).

The most common line ratios used in strong-line methods are summarised in López-Sánchez et al. (2012). The most popular ones are R_{23} (Pagel et al., 1979; Maiolino et al., 2008), N_2 (Denicoló et al., 2002; Nagao et al., 2006) and O_3N_2 (Alloin et al., 1979; Pettini & Pagel, 2004; Marino et al., 2013) which are defined as

$$R_{23} \equiv \frac{[\text{OII}]\lambda 3727 + [\text{OIII}]\lambda 4959 + [\text{OIII}]\lambda 5007}{\text{H}\beta}$$

$$N_2 \equiv \log\left(\frac{[\text{NII}]\lambda 6584}{\text{H}\alpha}\right)$$

$$O_3N_2 \equiv \log\left(\frac{[\text{OIII}]\lambda 5007/\text{H}\beta}{[\text{NII}]\lambda 6584/\text{H}\alpha}\right)$$

R_{23} suffer from being two-valued with respect to metallicity with a low-metallicity and a high-metallicity branch and an ill-defined turnover region between the two. This is because a small value of R_{23} can either mean that there is little of the heavy element, or that there is relatively much such that the electron temperature is low suppressing collisional excitation. O_3N_2 uses the ratio of two forbidden-to-recombination line ratios with different turnover regions to avoid this issue. This method, however, has the issue that the [OIII] and [NII] lines used are at significantly different wavelengths, so that flux calibration and extinction correction becomes important. N_2 is not double valued, but flattens and saturates for high metallicities.

The conversion from line ratio to metallicity is complicated by the fact that the strong-line intensity also depends on the ionization parameter (i.e. the number of ionizing photons per particle), q, in addition to the metallicity. Empirical calibrations ignore this and simply gives the metallicity as a linear or polynomial function of the line ratio used. In contrast, it is natural to include q-dependent terms in theoretical methods, as q has to be input to the photoionization model anyway. q is usually estimated from $[\text{OIII}]\lambda 5007/([\text{OII}]\lambda 3726+[\text{OII}]\lambda 3729)$ although $([\text{SIII}]\lambda 9069+[\text{SII}]\lambda 9532)/([\text{SII}]\lambda 6717+[\text{SII}]\lambda 6731)$ is a more reliable indicator when available as it does not depend on metallicity (Kewley & Dopita, 2002). The q-dependence is less relevant for integrated galactic metallicities though as the metallicity will be averaged over a large amount of HII regions with different q in that case. A more sophisticated approach to converting line ratios to galactic metallicity is used in Tremonti et al. (2004). Their calibration is based on a wide array of strong lines which are all fit simultaneously to a model of integrated galaxy spectra, yielding a likelihood surface rather than a simple function between a line ratio and metallicity.

2.3 Stellar metallicities

For an individual field star, metallicity is estimated from the absorption lines in the spectrum by modeling the line formation process and stellar atmosphere. This is highly non-trivial, but some progress has been made in recent years by advancing from one-dimensional to three-dimensional models and abandoning the assumption of local thermal equilibrium (Asplund, 2005).

For determining the mean stellar metallicity of a galaxy, where individual stars typically cannot be resolved, a method called "Stellar Population Synthesis (SPS) modeling" is used. The mean metallicity, along with total stellar mass, mean stellar age and star formation history, is estimated by fitting a synthetic spectrum or spectral energy distribution (SED; when only photometry is available) to the observed one. The synthetic spectra/SEDs are generated in a series of steps described in detail in Conroy et al. (2009). First, isochrones, i.e. colour-magnitude tracks of stars of equal age, are calculated for each fitted stellar age. A spectrum is then assigned to each sampled point in the colour-magnitude diagram based on a library of spectra of different temperatures, surface gravities and metallicities. Such a library consists of either observed spectra or empirically calibrated spectra computed from a photospheric model. The composite spectrum of a stellar population of a given age, called a "Simple Stellar Population" (SSP), can then be found by integrating spectra along the corresponding isochrone, weighting by the IMF. The full synthetic galaxy spectrum for some age is then the sum of SSPs up to that age weighted by the star formation history and corrected for dust extinction.

SPS modeling has significant uncertainties, chiefly from poorly understood phases of stellar evolution such as the thermally pulsating AGB phase, the shape of the IMF in the turnover region about $M \sim 1M_{\odot}$ and variations in metallicity across the galaxy (Conroy et al., 2009). In addition, star forming galaxies have strong emission lines which must be subtracted from the spectra before SPS modeling can be used (Gallazzi et al., 2005).

3 Galaxy mergers

Mergers between galaxies are relatively rare in the local Universe but are believed to be essential to galaxy formation and evolution, as mergers can dramatically change the galaxies involved and are more common at higher redshift. In addition to mergers, galaxies can also interact quite strongly during close flybys, but the effects, time-scales and frequency of such flybys are at present very poorly constrained so I will focus on mergers in this section.

3.1 Effect of mergers on star formation and morphology

In numerical simulations of mergers it is found that a significant fraction of the gas in the disk of the primary galaxy falls towards the centre (Mihos & Hernquist, 1996; Hopkins et al., 2009). This severe infall event is associated with stellar and gas bars formed by the nonaxisymmetric perturbations caused by the secondary galaxy. The gas bar lags slightly behind the stellar bar because the gas is collisional while the stars are collisionless. This causes the stars to torque the gas, such that it loses angular momentum and falls inwards. As the rate of star formation generally increases with increasing gas density, (Kennicutt, 1998) this infall triggers a burst of star formation which can enhance the SFR by a couple of orders of magnitude. Cox et al. (2008) found that the efficiency of the starburst, defined as the SFR relative to the SFR of the same galaxy evolved in isolation, increased approximately linearly with mass ratio. In addition, the magnitude of the burst also increases with higher gas fractions and decreases with larger bulges because bulges stabilise disks against the perturbations that cause the infall. The orientation of the galaxies also matters, with retrograde encounters causing more star formation than prograde encounters because less gas is transferred between the galaxies in the retrograde case. This leaves more gas in the disk, where it is available for star formation (Di Matteo et al., 2007).

Interactions between galaxies can strongly affect their morphologies well before they actually merge (if they end up merging at all). The most dramatic example of this is the formation of tidal tails and "bridges" of material connecting the galaxies. The archetype of this class of interacting galaxy pairs is M51 (see Figure 1), which has led to them being called "M51-type pairs" (Buta, 2013). Another example is the formation of bars previously mentioned.

Figure 1: The interacting galaxy pair M51 (NASA – Photo in public domain).

Rings, inner disks and warped disks are very common and in most cases associated with internal dynamics, rather than interactions. However, inner disks and warped disks have been observed in some galaxies where their presence cannot be explained by internal processes, and for these galaxies mergers have been shown to be a viable explanation (Eliche-Moral et al., 2011). In addition, some rarer types of rings, namely accretion rings, polar rings and collisional rings, are thought to be signs of a recent merger (Buta, 2013). The defining feature of accretion rings is that they rotate opposite to the rest of the galaxy. These rings are formed from material accreted from a smaller satellite galaxy. A polar ring, as the name suggests, tends to be nearly perpendicular to the rest of the galaxy and is also associated with the accretion of a satellite. Collisional rings are thought to arise from galaxy collisions where one of the galaxies passes through the centre of the other. These rings are blue, luminous and sites of star formation (Appleton, 1999). A dramatic example is the "Cartwheel galaxy" which consists of a centre, an inner ring and a prominent outer ring connected to the inner ring by "spokes".

In general, mergers between spiral galaxies will tend to produce an elliptical galaxy. In fact, a popular hypothesis is that the majority of elliptical galaxies are formed in this way (Toomre, 1977). However, if the galaxies have

high gas fractions, feedback from star formation can pressurise the gas stabilising the disks against fragmentation such that the remnant ends up being a spiral galaxy, even in major mergers (Springel & Hernquist, 2005).

Aside from visual inspection, mergers can be discerned from other galaxies through various parameters. Many such merger indicators have been devised, these are described in detail in Lotz et al. (2004) and Conselice (2014). The asymmetry, A, of a galaxy is defined as the difference in pixel values between the image of the galaxy out to some radius and the same image rotated by some amount (typically 180 degrees). It is important to use a well-defined radius, as A is a strong function of radius (Conselice et al., 2000). Typical values of A vary by galaxy type, but are in general much higher for merging galaxies. The smoothness, S, is essentially measured by subtracting a blurred galaxy image from the normal image. The image of residuals produced in this way functions as a measure of how clumpy the distribution of the galaxy's light is, regardless of whether the clumps are near the center or further out. A common and simple merger criterion is $A > 0.35$ and $A > S$ Conselice (2014). Another parameter is the concentration, C, which is basically the ratio of the radius encompassing most of the galaxy's light (e.g. 80 per cent) and some radius containing less of the light (e.g. 20 per cent). Interacting galaxies tend to become more concentrated than when they were isolated because of the previously mentioned central starburst that occurs during a merger (Li et al., 2008). However, many isolated galaxies also have high concentration, so concentration is not by itself sufficient to classify galaxies as mergers. Two more sophisticated parameters are the Gini coefficient and M_{20}. The Gini coefficient measures the area between the cumulative luminosity distribution of the pixels, sorted from lowest to highest, and the cumulative distribution that the pixel luminosities would follow if each pixel was equally bright (i.e. a straight line). As such, it measures the clumpiness of the galaxy without having to subtract another image, as is necessary to compute A and S. M_{20} is the second order moment of the luminosity distribution of the brightest 20 per cent of the galaxy. Thus, it is also a measure of how concentrated the light is, but, in contrast with C, the light can be concentrated anywhere in the galaxy.

3.2 Merger-induced metallicity dilution

Spiral galaxies are found to have radial metallicity gradients with the metallicity decreasing exponentially (i.e. linearly in $\log(\mathrm{O/H})$ units) with galactocentric radius (Zaritsky et al., 1994; Luck & Lambert, 2011). This gradient is usually about -0.10 dex/kpc and is thought to be a consequence of "inside-out" disk formation, i.e. that parts of a galactic disk closer to the centre evolve faster than parts further away (Sánchez et al., 2014). As mentioned previously, during a merger substantial amounts of gas falls towards the centre of the primary galaxy. Because of the presence of metallicity gradients this gas from further out in the disk causes the gas in the more central regions to be diluted and the metallicity gradient to flatten.

In recent years, this metallicity dilution has been studied in hydrodynamical merger simulations, which have mostly been limited to 1:1 mergers. Rupke et al. (2010) found that the nuclear metallicity decreased by $0.1-0.3$ dex after the first pericentric passage in a 1:1 merger probing an array of different inclinations and retrograde/prograde combinations. These simulations did not include any stellar feedback (so there was no enrichment from star formation), however. More comprehensive simulations were performed by Montuori et al. (2010) who included stellar feedback and also looked at flybys in addition to mergers. In good agreement with Rupke et al. (2010), they found an average metallicity depression of $0.2 - 0.3$ dex, but the inclusion of stellar feedback caused the metallicity to eventually increase above its pre-merger level in most cases. Remarkably, they found that grazing flybys affected the metallicity in much the same way as mergers. They also found that the time between metallicity dilution becoming significant and the metallicity recovering to its pre-merger value was ~ 2 Gyr.

The most comprehensive numerical study of metal-induced metallicity dilution to date is Torrey et al. (2012). They probed different orientations, gas fractions, masses and mass ratios. They found that the average metallicity depression was about 0.07 dex. The reason for this value being smaller than other studies is the inclusion of mass ratios other than 1:1 as smaller mass ratios lead to the dilution being less severe. They also showed that while the orientation of the galaxies changed the magnitude of the dilution, the mean was well-behaved with a reasonably small dispersion. Gas fractions were found to be important with higher gas fractions causing less dilution. At very high gas fractions the merger might even lead to enrichment rather than dilution.

As previously mentioned, the infall of gas during a merger also leads to enhanced star formation and this has a substantial effect on the metallicity evolution. In addition to causing the metallicity to eventually recover after the merger, this star formation also causes the metallicity as a function of time to have a "double-dip" shape, which is seen in merger simulations that include star formation and feedback. After first pericentric passage the metallicity starts decreasing, but concurrently the SFR starts increasing and the metals ejected from these newly formed stars cause the metallicity to decrease at a slower rate and eventually begin to increase. Before it can fully recover, though, the trajectories of the galaxies start bringing them closer which, once again, disturbs the primary galaxy inducing dilution and star formation, and the metallicity drops to a lower level than during the first passage. Shortly after the second passage the galaxies finally coalesce and the metallicity keeps recovering eventually surpassing its pre-merger value. Given sufficient time without another interaction event the remnant galaxy will presumably settle on a new equilibrium between gas flows and star formation and follow the stellar mass-SFR-metallicity relation (assuming that this relation is the consequence of such an equilibrium state, see §4.3). This scenario can be seen in the merger simulation of Scudder et al. (2012) shown in Figure 2.

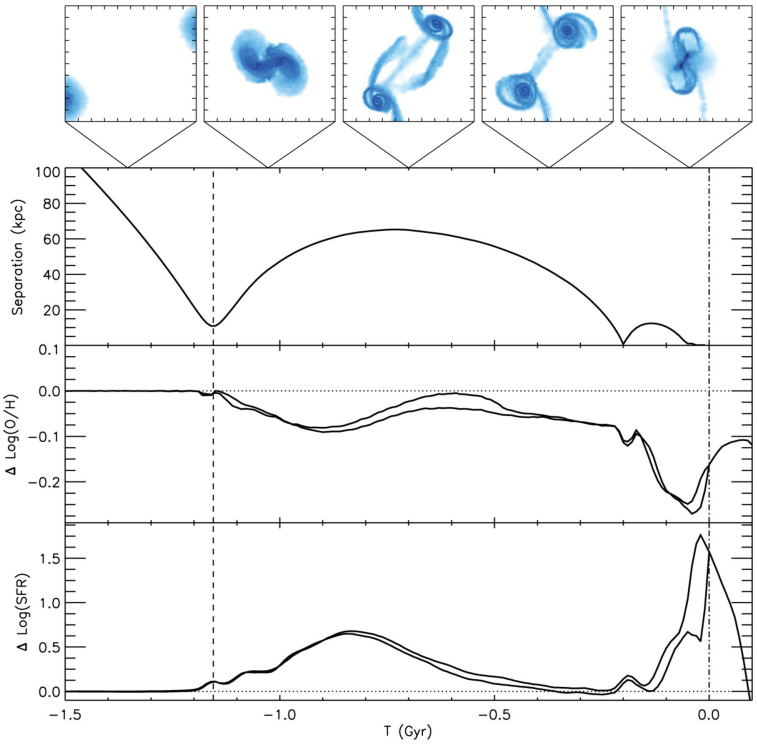

Figure 2: Evolution of the metallicities and SFRs of two merging galaxies of equal masses simulated in Scudder et al. (2012).

Observational studies of close galaxy pairs find metallicity depressions of typically about 0.05 dex (Ellison et al., 2008b; Michel-Dansac et al., 2008; Scudder et al., 2012). This is smaller than what is found in simulations of 1:1 mergers, but this is expected as these observational studies include galaxies down to mass ratios of about 1:10, so the results are still compatible. In addition to the magnitude of the dilution, Michel-Dansac et al. (2008) found that the secondary merger members showed enhanced metallicities, rather than dilution, and Ellison et al. (2008b) found that galaxies with small half-light radii appeared to be more strongly affected than larger galaxies.

3.3 The merger rate

The frequency of galaxy mergers can be estimated either from observations or simulations, both of which are notoriously difficult. The merger rate is usually defined as the number of mergers (often divided by the total number of galaxies to get the merger probability, i.e. mergers per galaxy) per time, R [Gyr^{-1}], or per comoving volume per time, Γ [Mpc^3 Gyr^{-1}]. The merger rate grows with increasing redshift, with R showing a strong redshift dependence and Γ a somewhat weaker one. While both observationally and theoretically derived merger rates have significant uncertainties, the observational major merger rates generally agree quite well with the theoretical ones. The total (minor+major) merger rate inferred from simulations, however, shows factor $\sim$ 3 discrepancies with the total merger rate from observations (Lotz et al., 2011).

3.3.1 Merger rates from observations

Observationally, merger rates can be estimated based on one of three methods – visual inspection, merger indicators (as described in §3.1) or close pairs. By counting the number of mergers in some volume the merger fraction, i.e. the fraction of galaxies at the observed redshift that are undergoing a merger, is found which can then be divided by the merger time-scale to obtain the merger rate at that redshift. Visual classification is problematic because its subjective nature makes comparisons to other merger rate estimates difficult. Instead, merger indicators such as asymmetry, A, and Gini coefficient, G, are often used. This is complicated by the fact that galaxies only show disturbed morphologies during some stages of a merger. The sum of these gives the "effective merger time-scale" that the merger fraction should be divided by to get the merger rate and this time-scale differs for each indicator. The mass ratio range that each indicator is sensitive to also differs, e.g. A typically identifies mergers with baryonic mass ratios down to about 1:4 while G and M_{20} identify mergers down to baryonic mass fractions of about 1:10 (Lotz et al., 2011). In addition, the time-scale and mass ratio ranges of each indicator also depends on the gas fractions of the merging galaxies, e.g. A is able to also detect minor mergers when the gas fractions are high. Because gas fractions generally increase with redshift this means that the mean merger time-scale and mass ratio range for each indicator is a function of redshift.

Using close galaxy pairs instead avoids the complication of only being sensitive to mergers at certain disconnected stages, but misses mergers that have almost coalesced and therefore are mistaken to be a single galaxy by the algorithm employed. Pairs are identified as galaxies that are close in redshift and within some projected distance (typically ~ 30 kpc) of each other and have relative velocities below some threshold (typically ~ 500 km s^{-1}). Both methods based on close pairs and on merger indicators tend to produce numerous false positives and will therefore overestimate the merger rate if this is not corrected for. Close pairs mistake some flybys for mergers, and merger indicators mistake some galaxies which have disturbed morphologies because of internal processes, such as disk instabilities, as being mergers. In either case the correction factor is ~ 0.6 (Lotz et al., 2011).

3.3.2 Merger rates from simulations

Alternatively, the merger rate can be inferred from simulations. This method has the advantage of being able to derive the merger rate as a function of mass ratio and primary galaxy mass rather than just the total major or minor merger rate found observationally. However, it is not yet possible to run sufficiently large simulations to directly estimate the galaxy-galaxy merger rate. Instead, the galaxy-galaxy merger rate is derived from the halo-halo merger rate from cosmological dark matter simulations such as the Millennium Simulation. These halo-halo merger rates have uncertainties associated with the algorithm used to identify mergers, resolution limits and the cosmological parameters. Nevertheless, most of the uncertainty comes from the conversion of the merger rates from halo-halo to galaxy-galaxy. A merger between halos is not the same as a merger between galaxies as the smaller halo will spend considerable time as a subhalo inside the bigger halo before the galaxies within the halos themselves merge. Ideally, this is taken into a account by following the subhalos until they fully merge, but this is often not feasible in which case a merger delay time is added. Even when subhalos are being followed, a "hybrid" approach often has to be used where the estimated merger time remaining is added once the subhalo comes too close to the primary galaxy to be distinguished in the simulation. The merger time can be estimated from merger simulations (e.g. Lotz et al. (2008)), analytical or numerical calculations of characteristic time-scales for gravitational or angular momentum capture (see Hopkins et al. (2010b)), or analytical calculations based on dynamical friction (e.g. Boylan-Kolchin et al. (2008)).

In addition, the halo masses and halo mass ratios must be converted to another type of mass more appropriate for galaxies to be useful. Typically, stellar mass is used because stellar masses are relatively widely available through the fitting of stellar population synthesis models (see §2.3). The stellar mass is a poor proxy for the total mass involved in mergers at low masses and high redshifts, where gas fractions are high, though. In this case, Hopkins et al. (2010a) recommends using the total tightly bound mass of the galaxies (defined there as the sum of stellar mass, gas mass and halo dark matter mass within 3 effective radii), if available. In any case, though, halo mass ratios are very poor proxies for stellar mass ratios because the halo mass – stellar mass relation, while being

one-to-one, is far from being a straight line. It rises sharply for low masses, but there is a "knee" at halo mass $M_h \approx 10^{12} M_\odot$ after which the relation becomes much shallower (Behroozi et al., 2010). Because of this, a 1:3 halo mass ratio might correspond to a 1:9 stellar mass ratio at low galaxy masses, but a 1:2 stellar mass ratio at high galaxy masses.

Ideally, the merger rate from simulations should be able to correctly predict the observational major, minor and total merger rates. As previously mentioned though, there is a significant discrepancy between the total merger rates. In principle, this discrepancy can be used to gain insight into problems with models of galaxy evolution and cosmology.

4 The mass-metallicity relation and second-parameter dependencies

4.1 The mass-metallicity relation

A relation between galaxy stellar mass and gas metallicity was first noted by Lequeux et al. (1979). Instead of mass, luminosity has often been used (in fact a relation between the luminosity and metallicity of elliptical galaxies had been found previously by McClure & van den Bergh (1968)), but in recent years stellar masses have become much more widely available through the fitting of stellar population synthesis models. In the seminal paper of Tremonti et al. (2004) the mass-metallicity relation (MZR) was derived using a sample of 53,000 local SDSS galaxies and a sophisticated method of estimating metallicity (see §2.2.2). Although the shape of the MZR differs greatly across different metallicity calibrations (Kewley & Ellison (2008), see Figure 3), a strong positive correlation between mass and metallicity that is steepest at low masses and flattens at high masses and is well described by a simple polynomial is generally found. The scatter about the relation is typically in the range $0.08 - 0.13$ dex at low redshift (Kewley & Ellison, 2008).

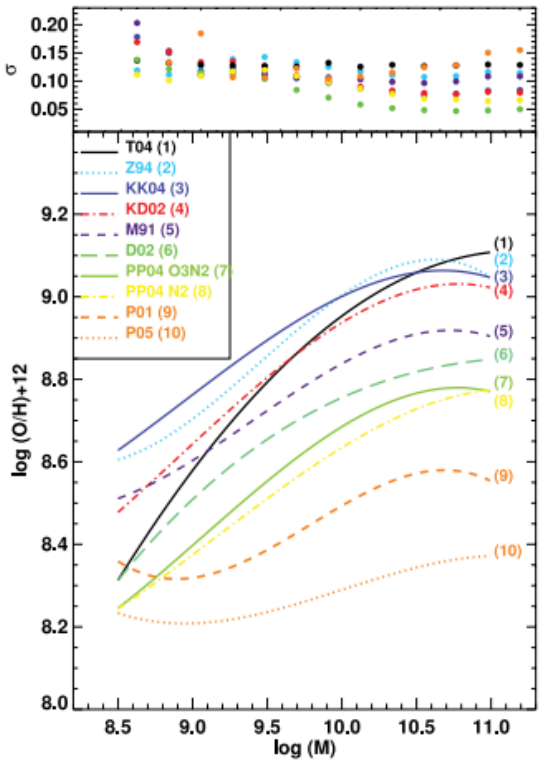

Figure 3: Best-fit mass-metallicity relations for a range of different metallicity calibrations, after Kewley & Ellison (2008). The top panel shows the RMS scatter around the relations in bins of 0.1 dex in mass.

The MZR can be explained by outflows being more effective at driving metals out in smaller galaxies because of their shallower gravitational potential wells (Dekel & Silk, 1986; Tremonti et al., 2004; Finlator & Davé, 2008). In the model of Dekel & Silk (1986) the outflow velocity is constant, but Finlator & Davé (2008) argued that this led to an MZR that was in conflict with observations and used an outflow velocity that was proportional to the halo velocity dispersion instead. Alternatively, the MZR may be the result of a variable Initial Mass Function (IMF) where massive galaxies are more efficient at producing massive stars than smaller galaxies (Köppen et al., 2007), or low-mass galaxies being generally less efficient at turning gas into stars (Brooks et al., 2007). The MZR appears to be part of a mass-SFR-metallicity relation though, which is typically explained by a combination of inflows and outflows (see §4.3).

4.2 Redshift, environment and SFR dependencies

In addition to mass, metallicity is known to depend on redshift (Erb et al., 2006; Maiolino et al., 2008; Cullen et al., 2014), environment (Cooper et al., 2008; Ellison et al., 2009) and star formation rate (Ellison et al., 2008a; Lara-López et al., 2010; Mannucci et al., 2010). However, these trends are not well known quantitatively. There seems to be a redshift evolution with the MZR shifting downwards to lower metallicities with higher redshifts. Accurate determination of the MZR at high redshift ($z > 2$) is hampered by small sample sizes. At $z \approx 0.1$ the vast SDSS sample allows the local MZR to be determined using sample sizes of order 10^5 galaxies. In contrast, all studies of the MZR at $z > 2$ has used samples of less than 100 galaxies. Erb et al. (2006) was the first to measure the MZR at a high redshift. They found that the MZR at $z \approx 2.2$ was shifted downward by 0.56 dex compared to the local MZR of Tremonti et al. (2004). Maiolino et al. (2008) determined the MZR at $z \approx 3.5$ using a sample of just nine galaxies. They derived their own metallicity calibrations and were careful to convert metallicities from previous works to their calibrations when comparing MZRs at different redshifts. They found that their $z \approx 3.5$ galaxies

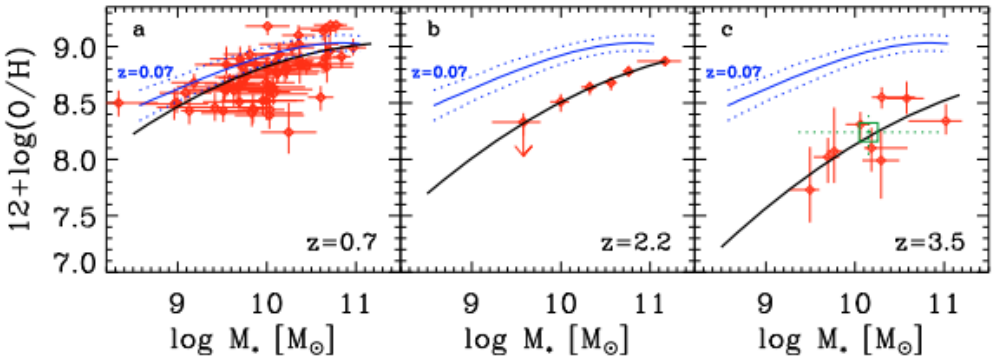

Figure 4: The redshift evolution of the mass-metallicity relation, after Maiolino et al. (2008). Left is the MZR at $z \approx 0.7$ from Savaglio et al. (2005), center is the MZR at $z \approx 2.2$ from Erb et al. (2006) and right is the MZR at $z \approx 3.5$ from Maiolino et al. (2008). The blue curve is the local MZR from Kewley & Ellison (2008).

followed an MZR that was shifted further towards low metallicities than the Erb et al. (2006) MZR (see figure 4). In a recent study by Cullen et al. (2014) an MZR with a significantly larger offset towards lower metallicities than Erb et al. (2006) was found despite the redshift range of the samples being approximately similar. Most studies, in addition to overall lower metallicities, also find that the offset is larger at low masses, i.e. the MZR steepens with redshift. A possible explanation for the redshift dependence of the MZR is that galaxies at higher redshifts simply have had less time to form massive stars to enrich their gas (Brooks et al., 2007). Alternatively, if the MZR is actually part of a largely redshift-independent mass-SFR-metallicity relation as suggested by many recent studies (see §4.3), it follows that the redshift evolution of the MZR is just a consequence of the redshift evolution of the stellar mass-SFR relation (Davé, 2008).

Local environment has also been found to affect the metallicity of galaxies. Galaxies in overdense regions have slightly higher metallicities than the general population (Cooper et al., 2008; Ellison et al., 2009). These tend to reside in clusters, but it is the high density, rather than cluster membership by itself, which is found to lead to higher metallicities. This is theorised as being caused by either ram pressure and tidal stripping or starbursts. Gas stripping can increase the metallicity of a galaxy by removing mostly metal-poor gas from the outskirts, or simply because the metal-rich matter ejected through recent SNe will constitute a larger fraction of the gas in a galaxy that has experienced gas stripping at an earlier point. In addition, the stripped gas can then enrich the IGM, such that the inflow of cluster galaxies will have less of a diluting effect on the galaxy. Alternatively, galaxies might experience a starburst when they enter a dense region causing their metallicity to increase.

The dependence on SFR was first examined by Ellison et al. (2008a). They found that galaxies with masses $M_* < 10^{10} M_\odot$ and small specific SFRs (SSFR$\equiv$ SFR$/M_*$) tend to have higher metallicities than the median for their mass, while high-SSFR galaxies show the opposite trend. This was also found in Lara-López et al. (2010) who fitted a plane to the mass-SFR-metallicity distribution. The origin of this SFR dependence of the MZR is not completely clear, but the general result that metallicity depends on mass and SFR can be derived from crude models or scaling arguments. This is discussed in the next section.

4.3 The Fundamental Metallicity Relation

Mannucci et al. (2010) studied the SFR dependence of the MZR in more detail using a large sample of local SDSS galaxies. They binned stellar masses and metallicities by SFR and found that the MZR anticorrelated with the SFR bin for stellar masses below $10^{10.5} M_\odot$. This mass-metallicity-SFR relation can be fitted well by a polynomial of the form $\log(\text{O/H}) + 12 = a + bm + cs + dm^2 + es^2 + fms$ where $m \equiv \log(M_*/M_\odot) - 10$ and $s \equiv \log(\text{SFR})$. This relation was coined the *fundamental metallicity relation* (FMR). They found that the two-dimensional projection

that minimised the metallicity scatter had $\log(M_*) - \mu_{32}\log(\mathrm{SFR})$, where $\mu_{32} = 0.32$, as the abscissa, rather than just stellar mass. Curiously, they found no redshift evolution of the FMR up to $z \sim 2.5$. This result has been corroborated by later studies (Henry et al., 2013; Cullen et al., 2014). This suggests that the redshift evolution of the MZR is caused mainly by galaxies at higher redshifts having higher SFRs.

Mannucci et al. (2010) were able to reproduce μ_{32} from a "back-of-the-envelope" type calculation combining pristine infall, an outflow proportional to SFR and $1/M_*$ to some powers, and the Kennicutt-Schmidt law (Kennicutt, 1998). A relation between metallicity, mass and SFR is naturally produced in some simple analytical models (Lilly et al., 2013; Dayal et al., 2013; Forbes et al., 2014) where inflow and outflow both depend on SFR, and SFR is proportional to the gas mass. An important difference between these three models though is that the SFR dependence is caused by scatter in inflow rates in the Lilly et al. (2013) and Forbes et al. (2014) models, while Dayal et al. (2013) attributes the SFR dependence to differences in initial conditions. These models also predict little or no redshift evolution. The stellar mass-SFR-metallicity relation might be the consequence of a more fundamental stellar mass-HI mass-metallicity relation as studied in Bothwell et al. (2013). They found a correlation with metallicity to be present for all atomic hydrogen masses in contrast with the SFR correlation, which flattens at high masses and disappears altogether for $M_* > 10^{10.5} M_\odot$. However, SFRs as measured through Hα are available for a much larger amount of galaxies than the mass of atomic hydrogen, so currently the FMR is much more useful than the relation based on HI mass.

5 Summary of the project

As mentioned in the introduction, mergers are known to dilute the central metallicities of primary galaxies (a "primary galaxy" being the most massive member of a merging galaxy pair). Even though the Fundamental Metallicity Relation (FMR) is thought to be a product of gas flows, no studies have as of yet looked at what insight into the effect of mergers on metallicity might be obtained through the scatter of the FMR. In Mannucci et al. (2010) it was noted that the scatter around the FMR closely follows a normal distribution except for a slight overabundance of galaxies with lower metallicity than expected. They theorised that this could be due to galaxy mergers, but did not examine it any further. The purpose of my thesis project was to examine if this extended wing in the metallicity residuals of the FMR towards low metallicities could be accounted for by a simple analytical model based on merger-induced metallicity dilution and if so what this would imply about the impact and time-scale of such dilution events.

In the model I assume that the residuals $r \equiv (\log(\text{O/H})_{\text{data}}) - (\log(\text{O/H})_{\text{FMR}})$ would follow a normal distribution in the absence of mergers. This normal distribution is fitted in a two-step process: First a Gaussian function is fitted over the entire range, then a new Gaussian is fitted within two standard deviations of the mean. This is to ensure that the fit is not affected by the tails. The standard deviation and mean of this Gaussian is then inputted as fixed parameters in the merger model.

The merger model itself has three free parameters: τ, α and ξ_{min}. Mergers with a stellar mass ratio, i.e. the ratio between the primary (larger) galaxy mass and the secondary (lower) galaxy mass, greater than ξ_{min} dilute the metallicity of the primary galaxy by an amount proportional to the mass ratio. The constant of proportionality is the parameter α, i.e. the change in metallicity will be $\Delta r = \Delta Z = -\alpha\xi$. Here we assume that the change in residual metallicity is caused purely by the change in metallicity rather than changes in mass or SFR, an assumption we found to be quite accurate. This dilution remains constant for a time τ (in Gyr, i.e. billions of years), after which the metallicity immediately goes back to follow the intrinsic Gaussian scatter of the FMR.

The model depends on the merger rate and the distribution of galaxy stellar masses. I used the merger rate of Fakhouri et al. (2010), which I had to convert from using halo masses and redshift to stellar masses and lookback time.

To fit the model I of course needed a histogram of metallicity residuals which meant fitting an FMR to a large sample of galaxies. I used a subset of the Sloan Digital Sky Survey Data Release 9 (SDSS DR9) catalogue by the MPA-JHU group. I selected $\sim 167,000$ out of the total of ~ 1.8 million galaxies in this catalogue using criteria that were close to those employed in Mannucci et al. (2010). These criteria chiefly filtered out high-redshift galaxies, galaxies with active nuclei (AGNs) and galaxies with low signal-to-noise emission lines. The median redshift of the final sample was $z = 0.11$. Total stellar masses were available in the catalogue while the SFRs within the 3 arcsec aperture used by SDSS were derived from the extinction corrected Hα flux. Metallicities were found using the O3N2 calibration of Marino et al. (2013).

Once I had selected the sample, I fitted an FMR to the data and created a histogram of the metallicity residuals using 100 equally spaced bins from -0.5 dex to 0.5 dex. I found that, as in Mannucci et al. (2010), there was a significant tail towards lower metallicities. There was also a slight excess of galaxies with higher than predicted metallicities. I fitted a Gaussian to the entire distribution and defined the tail as all bins below two standard deviations from the mean. Examining the galaxies in this tail, I found that they had slightly lower stellar masses, higher specific SFRs (SFR/M_*), lower metallicities and smaller half-light radii than the general population. They thus form a physically distinct population. The higher SSFRs can be interpreted as galaxies in the tail experiencing a boost in SFR because they are interacting.

I fitted 40^3 models (40 values of each free parameter equally spaced) to the histogram of residuals evaluating the goodness-of-fit of each model as the log-likelihood for poisson distributed errors. I found the best-fitting parameters to be $\tau = 1.79^{+0.046}_{-0.042}$ Gyr, $\alpha = 0.2095^{+0.0016}_{-0.0019}$ and $\xi_{\text{min}} = 0.3200^{+0.0149}_{-0.0135}$. The errors are statistical errors only, i.e. they are the uncertainties that arise from slightly different parameter values being almost equally good at fitting the data, but do not include uncertainties in the underlying measurements (e.g. the SFRs), the assumptions of the model, etc.

The best-fitting value of α leads to an average decrease in metallicity of about 0.2 dex during a 1:1 merger. This is in good agreement with simulations (Montuori et al., 2010; Rupke et al., 2010). The average decrease in metallicity during the mergers included in the model, i.e. mergers with $\xi > \xi_{\text{min}} = 0.32$ so essentially all major mergers, was 0.116 dex. This is a factor of ~ 2 larger than what is found in the observational studies of galaxy pairs of Ellison et al. (2008b), Michel-Dansac et al. (2008) and Scudder et al. (2012), but most of this discrepancy can be explained by these studies having minimum mass ratios smaller than 0.32. The best-fitting value of τ means that on average the metallicity remains depressed due to a merger for about 1.8 Gyr. This is in agreement with the ~ 2 Gyr of Montuori et al. (2010) and above the upper limit of 1 Gyr found in Torrey et al. (2012).

The main uncertainties of the model overall are the merger rate, which has an uncertainty of at least a factor of ~ 2 (Hopkins et al., 2010a), and the exclusion of flybys, which may be as common as mergers (Sinha & Holley-Bockelmann, 2012). In addition, a large source of uncertainty is the calibration used to determine the metallicities of the galaxies in the sample. The shape of the residual distribution varies with the calibration used, however the basic shape of a Gaussian with a significant tail towards low metallicities appears to be robust, as I found that it was present when using the popular calibrations of N2 from (Denicoló et al., 2002) and R23 from (Maiolino et al., 2008) in addition to the O3N2 calibration. There is also a potential uncertainty caused by ignoring secondary merger members, but in most cases the secondary galaxy should experience enrichment rather than dilution as it accretes gas from the more massive, and thereby typically more metal-rich, galaxy.

Aperture effects is a potential problem as the SFRs and metallicities were only measured within the 3 arcsec aperture used in SDSS. Although the redshift range in the sample is small ($z = 0.07$ to $z = 0.3$), the aperture on average covers a significantly larger part of the most distant galaxies than it does for the nearest ones. Additionally, there is also the aperture effect of galaxies with smaller radii being more completely covered on average than larger ones. Splitting the sample into a low-redshift and a high-redshift sample and finding the best-fitting model to these, I found that α was nearly unchanged while ξ_{min} was about 30 per cent higher and τ about 67 per cent lower for the high-redshift sample than for the low-redshift sample. The increase of ξ_{min} with redshift is expected as it represents the smallest merger that can cause a change in metallicity sufficiently large to be discernible from the Gaussian scatter in the FMR and this scatter grows with redshift as the masses, SFRs and metallicities become more uncertain. The decrease in τ with redshift may be mainly due to the increase in ξ_{min} with redshift if the dilution time-scale decreases with mass ratio as the merger time does (Hopkins et al., 2010b).

6 Conclusions and future work

In this thesis I have investigated the phenomenon of merger-induced metallicity dilution through a model of the scatter of the Fundamental Metallicity Relation (FMR). I selected a sample of $\approx 167,000$ galaxies from the SDSS and reproduced the tail towards lower metallicities in the scatter of the FMR noted by Mannucci et al. (2010). I showed that the tail is robust to the choice of metallicity calibration and forms a distinct population of galaxies that is consistent with being merging or recently merged galaxies.

I developed a simple model based on the hypothesis that the undisturbed galaxies follow a Gaussian scatter about the FMR, while the tail consists of merging galaxies. This model provides an excellent fit to the observed scatter which yields insights into the metallicity dilution associated with mergers. These predictions are in good agreement with the existing knowledge from merger simulations and observations of close galaxy pairs.

I find that an equal-mass merger on average leads to a metallicity depression of about 0.2 dex, in agreement with the hydrodynamical merger simulations of Montuori et al. (2010) and Rupke et al. (2010). I find that only mergers with mass ratio $\xi_* > 0.32$ lead to sufficient dilution to be discerned from the Gaussian scatter in the FMR. This closely corresponds to "major" mergers, which are often defined as mergers with mass ratio greater than 1:3. The average metallicity depression of all these major mergers is 0.116 dex, which is consistent with the actual metallicity difference of the tail compared to the entire sample. This is a greater dilution than what is found in the metallicity measurements of SDSS pair samples of Ellison et al. (2008b), Scudder et al. (2012) and Michel-Dansac et al. (2008), but my value is consistent with those studies when the differences between the minimum mass ratios in those samples and in our model are taken into account. I find that the metallicity on average stays depressed for 1.79 Gyr in good agreement with the merger simulations of Montuori et al. (2010).

The model can be improved in the future, as the two largest uncertainties stem from uncertainties in the merger rate and neglecting flybys. Incorporating flybys in the model was not possible as we currently have essentially no quantitative knowledge of flybys, but this should change in the future with further work based on the simple studies of Sinha & Holley-Bockelmann (2012) and Montuori et al. (2010), which were limited to grazing flybys. We would need to know with reasonable accuracy the flyby rate as a function of mass, mass ratio and pericentric distance; and how the dilution diminishes as the pericentric distance increases.

Furthermore, more comprehensive merger simulations are needed to test the model in more detail. Current works are all limited to 1:1 mergers, except for Torrey et al. (2012) who only includes a few mass ratios and just averages over them with no attempt at identifying trends with mass ratio. A simulation that included at least a reasonable range of major mergers and was run at least until the metallicity recovered would be able to test our assumption that the dilution, as time-averaged between pericentric passages, scales linearly with mass ratio. In addition, it could probe the relation between the dilution time-scale and mass ratio, which we assume to be independent. This assumption stems from our current lack of knowledge of this relation and some dependence on mass ratio is probable.

Our model makes some predictions that might be tested observationally. Low-metallicity outliers from the FMR should have a higher probability of being in a pair or showing disturbed morphology (e.g. higher asymmetry) than the general population. Also, a pair study where the pairs are binned by mass ratio should find that the median metallicity decreases as one moves towards larger mass ratio bins.

In addition, large-scale hydrodynamical simulations that track the metallicity of thousands of galaxies such as Illustris (Vogelsberger et al., 2014; Genel et al., 2014) or EAGLE (Schaye et al., 2015) should, in principle, enable a statistical study of merger-induced metallicity dilution. An FMR could be fit to the simulated galaxies, and if a low-metallicity tail appears in the scatter those galaxies could be directly checked for ongoing or recent interactions. The dilution time-scale, magnitude of metallicity depression and mass ratio dependence could then be inferred and compared with our results. This might not be possible with this first generation of large-scale hydrodynamical simulations though, as EAGLE has trouble reproducing the mass-metallicity relation (Schaye et al., 2015).

References

Alloin, D., Collin-Souffrin, S., Joly, M., & Vigroux, L. 1979, A&A, 78, 200

Andrews, B. H., & Martini, P. 2013, ApJ, 765, 140

Appleton, P. N. 1999, IAU Symposium, Vol. 186, Collisional Ring Galaxies, ed. J. E. Barnes & D. B. Sanders, p. 97

Asplund, M. 2005, ARA&A, 43, 481

Behroozi, P. S., Conroy, C., & Wechsler, R. H. 2010, ApJ, 717, 379

Bothwell, M. S., Maiolino, R., Kennicutt, R., Cresci, G., Mannucci, F., Marconi, A., & Cicone, C. 2013, MNRAS, 433, 1425

Bouché, N., Murphy, M. T., Kacprzak, G. G., Péroux, C., Contini, T., Martin, C. L., & Dessauges-Zavadsky, M. 2013, Science, 341, 50

Boylan-Kolchin, M., Ma, C.-P., & Quataert, E. 2008, MNRAS, 383, 93

Brooks, A. M., Governato, F., Booth, C. M., Willman, B., Gardner, J. P., Wadsley, J., Stinson, G., & Quinn, T. 2007, ApJ, 655, L17

Busso, M., Gallino, R., & Wasserburg, G. J. 1999, ARA&A, 37, 239

Buta, R. J. 2013, Galaxy Morphology, ed. T. D. Oswalt & W. C. Keel, p. 1

Coc, A., Vangioni-Flam, E., Descouvemont, P., Adahchour, A., & Angulo, C. 2004, ApJ, 600, 544

Conroy, C., Gunn, J. E., & White, M. 2009, ApJ, 699, 486

Conselice, C. J. 2014, ARA&A, 52, 291

Conselice, C. J., Bershady, M. A., & Jangren, A. 2000, ApJ, 529, 886

Cooper, M. C., Tremonti, C. A., Newman, J. A., & Zabludoff, A. I. 2008, MNRAS, 390, 245

Cox, T. J., Jonsson, P., Somerville, R. S., Primack, J. R., & Dekel, A. 2008, MNRAS, 384, 386

Cullen, F., Cirasuolo, M., McLure, R. J., Dunlop, J. S., & Bowler, R. A. A. 2014, MNRAS, 440, 2300

Davé, R. 2008, MNRAS, 385, 147

Davé, R., Finlator, K., & Oppenheimer, B. D. 2011, MNRAS, 416, 1354

Dayal, P., Ferrara, A., & Dunlop, J. S. 2013, MNRAS, 430, 2891

Dekel, A., & Silk, J. 1986, ApJ, 303, 39

Denicoló, G., Terlevich, R., & Terlevich, E. 2002, MNRAS, 330, 69

Di Matteo, P., Combes, F., Melchior, A.-L., & Semelin, B. 2007, A&A, 468, 61

Eliche-Moral, M. C., González-García, A. C., Balcells, M., Aguerri, J. A. L., Gallego, J., Zamorano, J., & Prieto, M. 2011, A&A, 533, A104

Ellison, S. L., Patton, D. R., Simard, L., & McConnachie, A. W. 2008a, ApJ, 672, L107

Ellison, S. L., Patton, D. R., Simard, L., & McConnachie, A. W. 2008b, AJ, 135, 1877

Ellison, S. L., Simard, L., Cowan, N. B., Baldry, I. K., Patton, D. R., & McConnachie, A. W. 2009, MNRAS, 396, 1257

Erb, D. K., Shapley, A. E., Pettini, M., Steidel, C. C., Reddy, N. A., & Adelberger, K. L. 2006, ApJ, 644, 813

Fakhouri, O., Ma, C.-P., & Boylan-Kolchin, M. 2010, MNRAS, 406, 2267

Finlator, K., & Davé, R. 2008, MNRAS, 385, 2181

Forbes, J. C., Krumholz, M. R., Burkert, A., & Dekel, A. 2014, MNRAS, 443, 168

Fryer, C. L. 1999, ApJ, 522, 413

Gallazzi, A., Charlot, S., Brinchmann, J., White, S. D. M., & Tremonti, C. A. 2005, MNRAS, 362, 41

Genel, S., et al. 2014, ArXiv e-prints, 1405.3749

Giavalisco, M., et al. 2011, ApJ, 743, 95

Henry, A., et al. 2013, ApJ, 776, L27

Hopkins, P. F., et al. 2010a, ApJ, 715, 202

Hopkins, P. F., Cox, T. J., Younger, J. D., & Hernquist, L. 2009, ApJ, 691, 1168

Hopkins, P. F., et al. 2010b, ApJ, 724, 915

Kennicutt, R. C., Jr. 1998, ARA&A, 36, 189

Kewley, L. J., & Dopita, M. A. 2002, ApJS, 142, 35

Kewley, L. J., & Ellison, S. L. 2008, ApJ, 681, 1183

Köppen, J., Weidner, C., & Kroupa, P. 2007, MNRAS, 375, 673

Lara-López, M. A., et al. 2010, A&A, 521, L53

Larson, R. B. 1972, Nature Physical Science, 236, 7

Lequeux, J., Peimbert, M., Rayo, J. F., Serrano, A., & Torres-Peimbert, S. 1979, A&A, 80, 155

Li, C., Kauffmann, G., Heckman, T. M., Jing, Y. P., & White, S. D. M. 2008, MNRAS, 385, 1903

Lilly, S. J., Carollo, C. M., Pipino, A., Renzini, A., & Peng, Y. 2013, ApJ, 772, 119

López-Sánchez, Á. R., Dopita, M. A., Kewley, L. J., Zahid, H. J., Nicholls, D. C., & Scharwächter, J. 2012, MNRAS, 426, 2630

Lotz, J. M., Jonsson, P., Cox, T. J., Croton, D., Primack, J. R., Somerville, R. S., & Stewart, K. 2011, ApJ, 742, 103

Lotz, J. M., Jonsson, P., Cox, T. J., & Primack, J. R. 2008, MNRAS, 391, 1137

Lotz, J. M., Primack, J., & Madau, P. 2004, AJ, 128, 163

Luck, R. E., & Lambert, D. L. 2011, AJ, 142, 136

Maiolino, R., et al. 2008, A&A, 488, 463

Mannucci, F., Cresci, G., Maiolino, R., Marconi, A., & Gnerucci, A. 2010, MNRAS, 408, 2115

Marino, R. A., et al. 2013, A&A, 559, A114

McClure, R. D., & van den Bergh, S. 1968, AJ, 73, 313

Michel-Dansac, L., Lambas, D. G., Alonso, M. S., & Tissera, P. 2008, MNRAS, 386, L82

Mihos, J. C., & Hernquist, L. 1996, ApJ, 464, 641

Montuori, M., Di Matteo, P., Lehnert, M. D., Combes, F., & Semelin, B. 2010, A&A, 518, A56

Nagao, T., Maiolino, R., & Marconi, A. 2006, A&A, 459, 85

Oppenheimer, B. D., & Davé, R. 2008, MNRAS, 387, 577

Osterbrock, D. E., & Ferland, G. J. 2006, Astrophysics of gaseous nebulae and active galactic nuclei

Pagel, B. E. J., Edmunds, M. G., Blackwell, D. E., Chun, M. S., & Smith, G. 1979, MNRAS, 189, 95

Pettini, M., & Pagel, B. E. J. 2004, MNRAS, 348, L59

Ramirez-Ruiz, E., Trenti, M., Roberts, L. F., Lee, W. H., & Saladino-Rosas, M. I. 2014, ArXiv e-prints

Rupke, D. S. N., Kewley, L. J., & Barnes, J. E. 2010, ApJ, 710, L156

Ryan, S. G., & Norton, A. J. 2010, Stellar Evolution and Nucleosynthesis

Sánchez, S. F., et al. 2014, A&A, 563, A49

Savaglio, S., et al. 2005, ApJ, 635, 260

Schaye, J., et al. 2015, MNRAS, 446, 521

Scudder, J. M., Ellison, S. L., Torrey, P., Patton, D. R., & Mendel, J. T. 2012, MNRAS, 426, 549

Sinha, M., & Holley-Bockelmann, K. 2012, ApJ, 751, 17

Smith, N. 2014, ARA&A, 52, 487

Springel, V., & Hernquist, L. 2005, ApJ, 622, L9

Stahler, S. W., & Palla, F. 2005, The Formation of Stars

Tinsley, B. M. 1980, Fund. Cosmic Phys., 5, 287

Toomre, A. 1977, Mergers and Some Consequences, ed. B. M. Tinsley & R. B. G. Larson, D. Campbell, p. 401

Torrey, P., Cox, T. J., Kewley, L., & Hernquist, L. 2012, ApJ, 746, 108

Tremonti, C. A., et al. 2004, ApJ, 613, 898

Vogelsberger, M., et al. 2014, ArXiv e-prints, 1405.2921

Willson, L. A. 2000, ARA&A, 38, 573

Wolfe, A. M., Gawiser, E., & Prochaska, J. X. 2005, ARA&A, 43, 861

Woosley, S. E., Heger, A., & Weaver, T. A. 2002, Reviews of Modern Physics, 74, 1015

Zaritsky, D., Kennicutt, R. C., Jr., & Huchra, J. P. 1994, ApJ, 420, 87

APPENDIX

Mon. Not. R. Astron. Soc. **000**, 000–000 (2014) Printed 28 November 2014 (MN LATEX style file v2.2)

Merging galaxies produce outliers from the Fundamental Metallicity Relation

Asger E. Grønnow⋆[1], Kristian Finlator[1] and Lise Christensen[1]
[1] *Dark Cosmology Centre, Niels Bohr Institute, University of Copenhagen, Juliane Maries Vej 30, 2100 Copenhagen, Denmark*

Submitted to MNRAS

ABSTRACT
From a large sample of local SDSS galaxies we find that the Fundamental Metallicity Relation (FMR) has an overabundance of outliers, compared to what would be expected from a Gaussian distribution of residuals, with significantly lower metallicities than predicted from their stellar mass and star formation rate (SFR). This low-metallicity population has lower stellar masses, enhanced specific SFRs and smaller half-light radii than the general sample and are hence a physically distinct population. We show that they are consistent with being galaxies that are merging or have recently merged with a satellite galaxy. In this scenario, low-metallicity gas flows in from large radii, diluting the metallicity of star-forming regions and enhancing the specific SFR until the inflowing gas is processed and the metallicity has recovered. We introduce a simple model in which mergers with a mass ratio larger than a minimum dilute the central galaxy's metallicity by an amount that is proportional to the stellar mass ratio for a constant time, and show that it provides an excellent fit to the distribution of FMR residuals. We find the dilution time-scale to be $\tau = 1.79^{+0.046}_{-0.042}$ Gyr, the average metallicity depression caused by a 1:1 merger to be $\alpha = 0.2095^{+0.0016}_{-0.0019}$ dex and the minimum mass ratio merger that can be discerned from the intrinsic Gaussian scatter in the FMR to be $\xi_{\rm min} = 0.3200^{+0.0149}_{-0.0135}$ (these are statistical errors only). From this we derive that the average metallicity depression caused by major merger is 0.116 dex.

Key words: galaxies: abundances – galaxies: interactions – galaxies: evolution

1 INTRODUCTION

Understanding the way that the metallicities of galaxies depend on galactic properties and events is crucial in understanding galaxy evolution as metallicity is connected to important galactic processes such as inflows, outflows and star formation. A relation between galaxy mass and metallicity was found in Lequeux et al. (1979) and measured to great accuracy based on SDSS Data Release 2 as a tight relation between galaxy stellar mass and gas-phase metallicity by Tremonti et al. (2004). This mass-metallicity relation (MZR) is thought to arise from galactic winds being more efficient at blowing metals out of lower mass galaxies owing to their shallower gravitational potential wells. The MZR depends on environment (Cooper et al. 2008) and redshift (Erb et al. 2006; Maiolino et al. 2008; Henry et al. 2013). In addition Ellison et al. (2008a) found that galaxies with high star formation rates (SFR) showed systematically lower metallicities than galaxies with similar masses but lower SFRs. This was studied in more detail in Mannucci et al. (2010) (hereafter M10) who binned stellar masses and metallicities by SFR and found that the MZR anticorrelated with the SFR bin for masses $M_* < 10^{10.5} M_\odot$. In light of this M10 introduced the Fundamental Metallicity Relation (FMR) between stellar mass, SFR and gas-phase metallicity. They interpreted the SFR dependence as being due to continuous accretion of pristine gas from the intergalactic medium raising the SFR while diluting the metallicity. Concurrently with M10 Lara-López et al. (2010) also investigated the SFR dependence of the MZR and also found a relation between mass, SFR and metallicity. These studies of second-parameter dependencies of the MZR all look at galaxy samples that are selected to differ with the parameter of interest whose MZRs can then be compared. A complementary way of examining further dependencies of the MZR or FMR is to instead select galaxies with abnormally low or high metallicity for their masses (and SFR in the case of the FMR) and then check what the metallicity offset correlates with.

Peeples et al. (2009) analysed a sample of 42 metal-poor galaxy outliers from the MZR and found that all but two of those showed signs of interaction. More systematically, M10 produced a histogram of the residuals of the FMR i.e. the difference between the measured metallicity and the metallicity predicted by the FMR for each galaxy. These residuals closely followed a Gaussian distribution with the exception of an extended wing of galaxies with lower nuclear metallicities than predicted. There it was speculated

⋆ E-mail: agronnow@dark-cosmology.dk

that the bulk of these low-metallicity galaxies were interacting, but this was not examined further.

That interactions tend to dilute nuclear metallicities has been found both in observations of close galaxy pairs (Kewley et al. 2006; Ellison et al. 2008b; Michel-Dansac et al. 2008; Scudder et al. 2012) and in simulations of mergers (Montuori et al. 2010; Rupke et al. 2010; Perez et al. 2011; Torrey et al. 2012) with these authors finding systematic offsets from the MZR of up to a few tenths of a dex towards lower metallicities for merging galaxies. The standard explanation for this phenomenon is that the centre of the primary spiral galaxy experiences a period of strong inflow of gas from the outskirts of the galaxy. This inflow is driven by torques exerted by stars in bar instabilities created by the tidal interactions (Mihos & Hernquist 1996) and it will be metal deficient compared to the nuclear metallicity as spiral galaxies have radial abundance gradients with lower metallicities at larger radii (Zaritsky et al. 1994; Luck & Lambert 2011). The inflow also leads to an increase in star formation which causes the metallicity to eventually recover on a time-scale of a few Gyr (Montuori et al. 2010).

In this paper, we ask whether the population of star-forming galaxies whose metallicities are significantly below expectations based on the FMR can be readily interpreted within the context of a simple model for galaxy mergers that dilute the nuclear metallicity and boosts its star formation. In particular:
(1) Can the low-metallicity tail be successfully modeled as being due to mergers?
(2) Do the galaxies in the low-metallicity tail show complementary evidence of being in mergers?
(3) What does this imply about the impact of mergers on galaxies' gas reservoirs and the time-scale over which mergers have such an impact?

We will show that mergers readily account for the observed low-metallicity outliers. This enables us to estimate the time-scale and magnitude of merger-induced metallicity dilution in a novel way.

In §2 we describe our sample selection. In §3 we fit an FMR to our sample and examine the differences between the main sample and the tail. In §4 we review our merger model and in §5 we describe how we find the best-fitting parameters and their values. In §6 we discuss uncertainties and assumptions in our model and compare our results to observations and hydrodynamical simulations. Finally, we summarise our findings and avenues for future work in §7.

2 SAMPLE SELECTION

We need to establish a large sample of galaxies in order to investigate the tail in the residuals of the FMR. We used a subset of the Sloan Digital Sky Survey (SDSS) DR9 catalogue by the MPA-JHU group available at http://www.sdss3.org/dr9/algorithms/galaxy_mpa_jhu.php where the techniques used to measure emission lines and derive galaxy parameters are also summarised. Half-light radii were adopted from the SDSS-DR9 photometric table "PhotoObjAll". The full catalogue contains 1,843,205 galaxies from which we selected 167,086 galaxies according to the following criteria which were adopted from M10.

Only galaxies with redshifts within $0.07 < z < 0.30$ were selected to ensure that the 3 arcsec aperture of the spectroscopic fibre covered a significant part of the galaxies. We also demanded that Hα was detected at a signal-to-noise ratio of at least 25. This ensures a sufficiently high S/N of the N[II] λ6584 line that is used in many metallicity calibrations as well as making BPT diagram classification of the galaxies more accurate. We selected only galaxies classified as BPT class 1 (star-forming) or 2 (low S/N star-forming) filtering out AGNs and composite galaxies. Finally, we filtered out galaxies for which it was not possible to measure the [OIII]λ5007 line which is necessary to determine the metallicity using the O3N2 or R23 calibrations (see §3.1); this amounted to 0.4 per cent of the remaining sample.

Total stellar masses were taken from the MPA-JHU catalogue, these were calculated using the method of Kauffmann et al. (2003). Star formation rates were derived from the extinction corrected Hα flux using the calibration in Kennicutt (1998) (with extinctions measured from Balmer decrements). The masses were multiplied by 1.06 and the SFRs divided by 1.8 to scale them to a Chabrier IMF (Chabrier 2003). SFRs and metallicities were measured within the aperture only without any aperture correction.

3 DATA ANALYSIS

3.1 Fitting an FMR

We had to use a strong-line method to find the metallicities of the galaxies in our sample. These methods are calibrated by fitting the relationship between the ratio of two or more strong emission lines and metallicities inferred directly from electron temperatures of HII regions. While "direct" metallicities found from electron temperature measurements are more accurate, they have to be calculated from auroral lines that are very weak and can only be detected with sufficient signal-to-noise in the SDSS spectra by stacking (Andrews & Martini 2013). This is a problem as we need to be able to measure metallicities for single galaxies as we will be studying outliers. We chose to use the O3N2 calibration of Marino et al. (2013), which gives $12 + \log(\mathrm{O/H})$ as a linear function of O3N2$\equiv \log\left([\mathrm{OIII}]\lambda5007/\mathrm{H}\beta \times \mathrm{H}\alpha/[\mathrm{NII}]\lambda6584\right)$, to derive metallicities as this recent calibration is based on more extensive electron temperature data than older calibrations such as Pettini & Pagel (2004). M10 used an average of the N2 and R23 calibrations of Maiolino et al. (2008) but as we are interested only in the residuals, the differences in the absolute metallicities derived from different calibrations do not matter and the differences in the residual distributions are quite small (see §6.4). We fitted an FMR of the form introduced in M10 to the data using least squares. While M10 only fitted their FMR to galaxies with $M_* < 10^{9.1} M_\odot$, we did not include a mass cut. In Mannucci et al. (2011), where the FMR was extended down to $M_* \approx 10^{8.3} M_\odot$, it can be seen that the FMR for low-mass galaxies begins to deviate significantly from the extrapolation of the FMR of M10 at masses below $\sim 8.8 M_\odot$. Only 0.1 per cent of the galaxies in our sample has such low masses. Our fit yielded

$$(12 + \log(\mathrm{O/H})_{\mathrm{FMR}}) = 8.436 + 0.222m - 0.129s - 0.093m^2 + 0.088ms - 0.052s^2 \quad (1)$$

where $m \equiv \log(M_*) - 10$ and $s \equiv \log(SFR)$ and m and s are in units of $M_\odot$ and $M_\odot$ yr^{-1}, respectively. The residuals $r \equiv (12 + \log(\mathrm{O/H})_{\mathrm{data}}) - (12 + \log(\mathrm{O/H})_{\mathrm{FMR}})$ were then computed for all galaxies.

We show a histogram of these metallicity residuals in figure 1. This histogram has 100 equally spaced bins from -0.5 dex to 0.5 dex. 58 of the 167,087 galaxies, i.e. about 1 in 3000 galaxies,

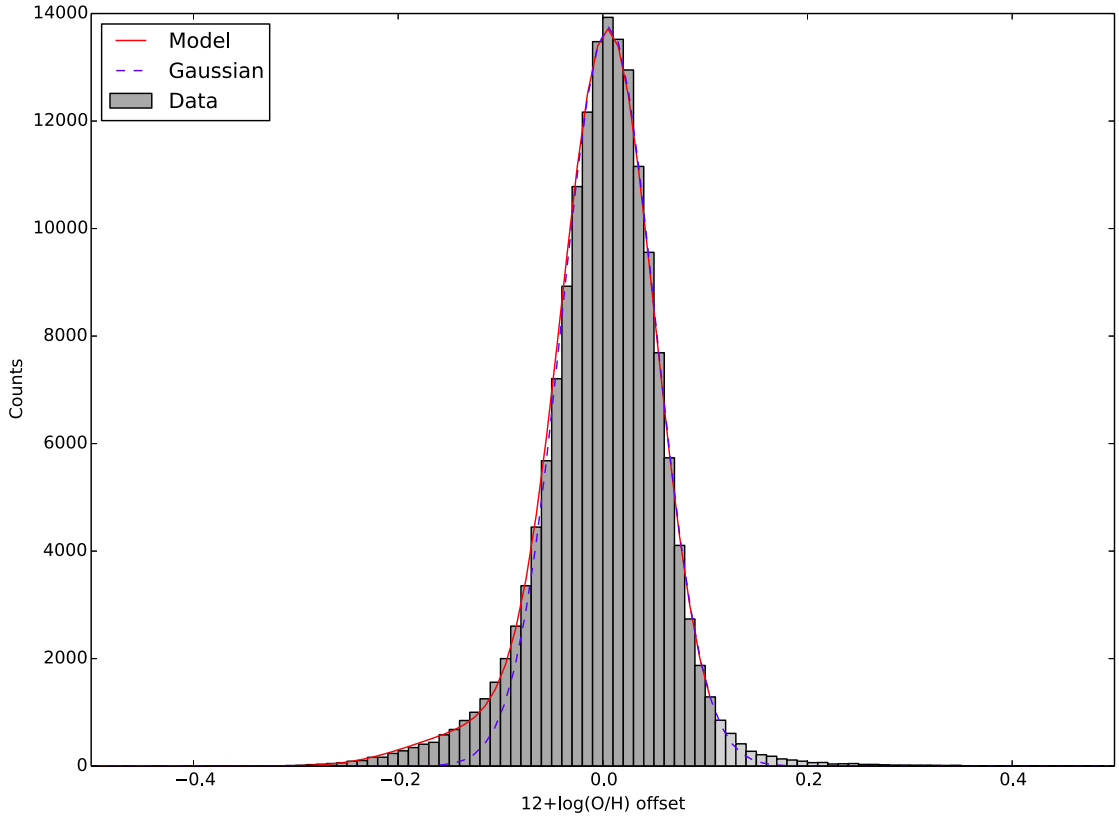

Figure 1. The gray histogram is the residuals of the fitted FMR, the unbroken line is the best-fitting model which has $\tau = 1.79$ Gyr, $\alpha = 0.2095$ and $\xi_{\rm min} = 0.32$ and the dashed line is the best-fitting Gaussian. The part of the histogram at large positive offsets that is in a lighter shade of gray is the high-r tail that is not included in the model.

fall outside this range. All but a single one of these outliers (which falls just below the range with $r = -0.5004$ dex) have $r > 0.5$ dex and appear to be mostly dwarfs with $\log(M_*/M_\odot) \sim 8$ and high specific SFRs. We will not examine these high metallicity outliers further and from this point on in the analysis these outliers are filtered out.

This metallicity dispersion is almost Gaussian distributed but with a distinct tail towards lower metallicities as was also noted in M10 (cf. their figure 3). We fit a Gaussian function to the metallicity dispersion using least squares finding a dispersion of $\sigma = 0.047$ dex and a slight offset from zero of $\mu = 0.005$ dex; this enables us to quantitatively define the tail as the bins with $r < \mu - 2\sigma$. This tail contains an excess amount of 4.29 per cent of all galaxies relative to the number of galaxies that it would contain if it followed the fitted Gaussian. Upon close inspection a tail towards high metallicities can be seen as well but this tail only contains an excess of about 1 per cent of all galaxies (where this tail is defined as the bins with $r > \mu + 2\sigma$).

M10 binned their stellar masses and SFRs in bins of 0.05 dex and then fitted their FMR to the median values in each bin. Doing this in our case turned out to make very little difference in the fitted FMR so we chose not to bin the masses and SFRs.

3.2 Properties of the galaxies in the tail

We compare the galaxies in the tail to the general population to establish whether or not they form a distinct population. The stellar masses of the galaxies in the tail are generally lower than the general population with a median value that is 0.26 dex below the median value of all galaxies, both being approximately lognormally distributed (see figure 2). This suggests that the tail cannot be an artefact of metallicity aperture effects alone (i.e. galaxies that are more completely covered by the aperture being found to have lower metallicities because of metallicity gradients) because in that case the mass distributions should be similar as the stellar masses are all estimated for entire galaxies. It also indicates that the tail is not predominantly driven by errors in mass because in that case the galaxies in the tail should have erroneously high masses as this would cause their predicted metallicities to be too high. That the galaxies in the tail have lower masses than the general population can be interpreted as being due to low-mass galaxies being more strongly impacted by mergers because of weaker bulges or higher gas fractions.

The specific SFRs (SSFR) of the galaxies in the tail are generally higher with a median value that is 0.30 dex above the median value for all galaxies (see figure 3) due to the median SFR being slightly higher even though the median stellar mass is lower. This indicates that the tail is not predominantly driven by errors in SFR because in that case the SFRs in the tail should have erroneously low SFRs as this would cause their predicted metallicities to be too high. A simple interpretation of the higher sSFRs in the tail is that many of those galaxies are experiencing a boost in star formation owing to interactions.

The metallicities of the galaxies in the tail are as expected sig-

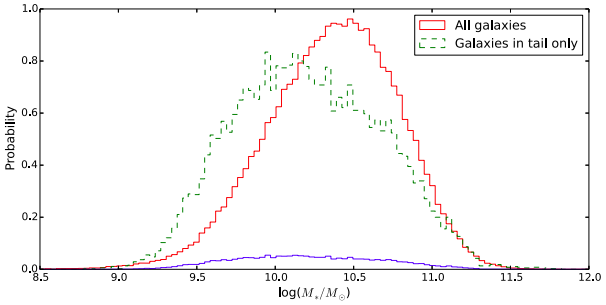

Figure 2. Histograms showing the normalised mass distribution of the overall sample (red) and only the galaxies in the tail (green, dashed). The blue curve is the mass distribution of the galaxies in the tail using the same normalisation as for the overall sample to compare the sample sizes.

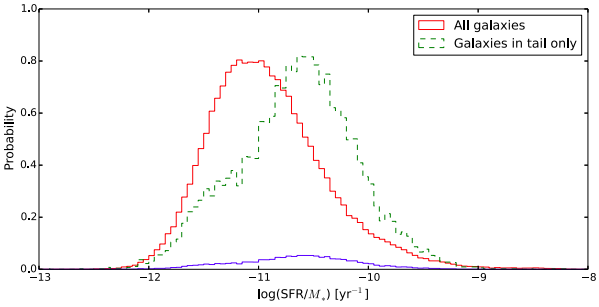

Figure 3. Same as figure 2 but for the specific SFR (SFR/M_*).

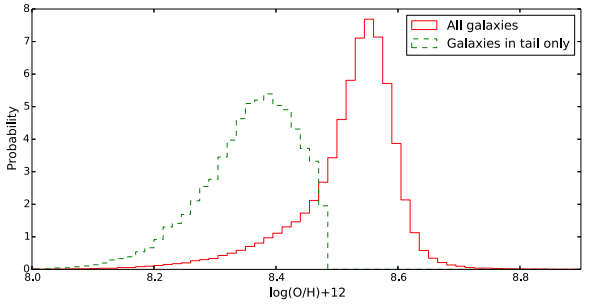

Figure 4. Same as figure 2 but for metallicity.

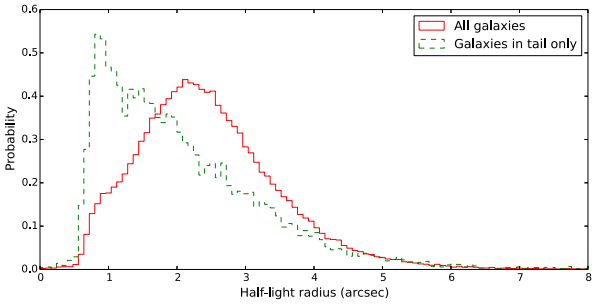

Figure 5. Same as figure 2 but for U-band half-light radii.

nificantly lower than for the general population the median metallicity of the tail being 0.17 dex below the overall median value (see figure 4). One might worry that a significant part of the tail would then have metallicities below $12 + \log(\mathrm{O/H}) = 8.2$, which is the lower limit of validity for the O3N2 calibration we use. However, only 4.4 per cent of the galaxies in the tail have metallicities below this. For the overall sample 99.2 per cent is within the range of validity of $8.2 < 12 + \log(\mathrm{O/H}) < 8.8$.

As can be seen in Figure 5, the galaxies in the tail have significantly smaller half-light radii than the general population. The figure shows the U-band half-light radii but the G and R bands show the same trend. The difference in the median values is about 30 per cent which is small enough that it could be attributed to the differences in the mass and redshift distributions (see §6.5) of the tail and general population samples. However, the sudden rise at 0.5 arcsec suggests that the half-light radii of many of these galaxies are overestimated because they are smaller than the seeing. Additionally, as can be seen from the figure, the modes of the two half-light radius distributions differ by a factor above 2. Thus a significant part of the galaxies in the tail are significantly more compact than is typical for the full sample. This is in agreement with Ellison et al. (2008b) who found that galaxies in their pair sample with half-light radii below 3 kpc tended to have lower metallicities than galaxies with larger half-light radii.

In summary, galaxies whose metallicity is lower than predicted for their stellar mass and SFR have systematically low stellar mass, high SSFR, small half-light radius and low metallicity. The offsets in SFR and stellar mass are the opposite of what would be expected if errors were driving galaxies into the tail. Also the tail towards lower metallicities is much larger than the tail towards higher metallicities. These considerations support the view that the low-metallicity tail consists of a physically distinct population.

4 THE MERGER MODEL

We assume that the residuals of the FMR in the absence of mergers would be a normal distribution and fit a Gaussian function to the residuals from the FMR found in §3.1 using least squares. A Gaussian $G(r)$ is then fitted again but this time only in the interval $[\mu - 2\sigma,\ \mu + 2\sigma]$, where the mean μ and the standard deviation σ is estimated from the first fit, in order to avoid the low-r tail where the shape deviates significantly from a Gaussian and the high-r tail which is not a part of the model. We then introduce a simple model to take the effect of interaction triggered metallicity dilution into account. This model has three free parameters, ξ_{min}, α and τ, and two fixed parameters namely the scatter and mean of the non-merging population $G(r)$ that has already been fitted.

Mergers above a certain mass ratio threshold ξ_{min} shift galaxies towards lower r by an amount $\alpha\xi_*$ where ξ_* is the stellar mass ratio of the merger with respect to the most massive galaxy. So in the case of a 1:1 merger the metallicity changes by $-\alpha$ dex assuming that the change in r caused by changes in stellar mass and/or SFR is small compared to the change in r caused by the metallicity change (we show that this assumption is quite accurate in §6.1). This offset remains constant for a time τ (in Gyr) before the galaxy's metallicity returns to normal i.e. goes back to follow the FMR. ξ_{min} can be thought of as representing the minimum shift in r that can be distinguished from the intrinsic Gaussian scatter of the FMR, so we would expect $\alpha\xi_{\mathrm{min}} \sim \sigma$.

The probability density function (PDF) of FMR residuals is

given by the following expression

$$P(r) = P(r|\text{unmerged})P(\text{unmerged}) + P(r|\text{merged})P(\text{merged}) \quad (2)$$

Obviously $P(\text{unmerged}) = 1 - P(\text{merged})$. $P(\text{merged})$ is calculated by integrating the merger rate per galaxy per mass ratio per lookback time for a galaxy of stellar mass M_*, $\frac{\mathrm{d}^2 P(\text{merged}|\xi_*, M_*)}{\mathrm{d}\xi_* \, \mathrm{d}t}$, over lookback times 0 to $T \gg \tau$, mass ratios from ξ_{min} to 1 (as ξ_* is defined as the stellar mass ratio of the merger with respect to the most massive galaxy) and the galaxy stellar mass PDF $\frac{\mathrm{d}P}{\mathrm{d}M_*}$.

$$P(\text{merged}) = \int_0^\infty \frac{\mathrm{d}P}{\mathrm{d}M_*} \int_{\xi_{\text{min}}}^1 \int_0^T \frac{\mathrm{d}^2 P(\text{merged}|\xi_*, M_*)}{\mathrm{d}\xi_* \, \mathrm{d}t} \frac{\tau}{T} \, \mathrm{d}t \, \mathrm{d}\xi_* \, \mathrm{d}M_* \quad (3)$$

$P(r|\text{unmerged})$ is just the normal distribution previously fitted to the data, $G(r)$, normalised to have unit area.

We calculate the second term in $P(r)$ by integrating the probabilities given a specific mass ratio over ξ_*.

$$P(r|\text{merged})P(\text{merged}) = \int_{\xi_{\text{min}}}^1 P(r|\text{merged}, \xi_*) P(\text{merged}, \xi_*) \, \mathrm{d}\xi_* \quad (4)$$

$P(r|\text{merged}, \xi_*)$ is just the Gaussian $P(r|\text{unmerged})$ where the mean is shifted from μ to $\mu - \alpha\xi_*$.

$$P(r|\text{merged})P(\text{merged}) = \int_0^\infty \frac{\mathrm{d}P}{\mathrm{d}M_*} \int_{\xi_{\text{min}}}^1 \int_0^T P(r|\text{merged}, \xi_*) \times \frac{\mathrm{d}^2 P(\text{merged}|\xi_*, M_*)}{\mathrm{d}\xi_* \, \mathrm{d}t} \frac{\tau}{T} \, \mathrm{d}t \, \mathrm{d}\xi_* \, \mathrm{d}M_* \quad (5)$$

We obtain the merger rate per galaxy per stellar mass ratio per lookback time from the merger rate per halo per halo mass ratio per redshift (for a halo mass M_h) $\frac{\mathrm{d}^2 P}{\mathrm{d}\xi_h \, \mathrm{d}z}(M_h, \xi_h, z)$ from Fakhouri et al. (2010) through the following calculation:

$$\begin{aligned} \frac{\mathrm{d}^2 P}{\mathrm{d}\xi_* \, \mathrm{d}t}(M_*, \xi_*, t) &= \frac{\mathrm{d}^2 P}{\mathrm{d}\xi_h \, \mathrm{d}z}(M_h, \xi_h, z) \frac{\mathrm{d}\xi_h}{\mathrm{d}M_{*,s}} \frac{\mathrm{d}M_{*,s}}{\mathrm{d}\xi_*} \frac{\mathrm{d}z}{\mathrm{d}t} \\ &= \frac{\mathrm{d}^2 P}{\mathrm{d}\xi_h \, \mathrm{d}z}(M_h, \xi_h, t(z)) \left. \frac{\mathrm{d}M_h(M_{*,s})}{\mathrm{d}M_{*,s}} \right|_{M_{*,s}} \times \\ &\quad \frac{M_*}{M_h(M_*)} (1+z) H_0 \sqrt{\Omega_M (1+z)^3 + \Omega_\Lambda} \end{aligned} \quad (6)$$

where $M_{*,s}$ is the stellar mass of the smaller galaxy in the merger and H_0 is in units of Gyr^{-1}. We use a ΛCDM cosmology with $H_0 = 70 \, \text{km} \, \text{s}^{-1} \, \text{Mpc}^{-1}$, $\Omega_\Lambda = 0.7$ and $\Omega_\text{m} = 0.3$ and the stellar mass - halo mass relation of Behroozi et al. (2010). Normally some "merger delay" time-scale would be imposed because a halo will spend some time as a subhalo before the merger is completed. We do not include this effect as the metallicity depression may well begin and end at different times than the merger itself as estimated from e.g. dynamical friction and operate on a time-scale that scales differently with parameters such as mass ratio from the merger delay time-scale (see §6.2).

We evaluate equation (2) numerically creating a histogram of galaxies in bins of width 0.005 dex in r. We do the time integration by simply multiplying by τ under the assumption that the merger rate is approximately constant over $T \gg \tau$ (i.e. assuming $T \ll t_H$ where t_H is the Hubble time) with the lookback time set to $t(z = 0.1) = 1.30$ Gyr, the typical redshift of the galaxies in our sample. The stellar mass integration is done by looping over 10 stellar masses equally logarithmically spaced from $\log(M_*/M_\odot) = 9.125$ to $\log(M_*/M_\odot) = 11.375$ with $\frac{\mathrm{d}P}{\mathrm{d}M_*}$ being based on the mass distribution of our sample. Finally, the probability is converted to galaxy counts in each bin in order to compare the model to the data.

5 MODEL FITS

We fit our 5-parameter model in two steps: First, we fit a Gaussian to the FMR residual distribution in the way described in §4. We found the best-fitting Gaussian had a mean of 0.006 dex and a scatter of 0.046 dex. Then we fitted the three parameters describing the low-r tail: ξ_{min} which represents the minimum mass ratio merger that can be discerned, α which represents the metallicity change caused by a merger and τ which represents the time-scale of the dilution (see §4 for a detailed description of these parameters). We ran 40^3 models with 40 equally spaced values of each of these.

We evaluate the relative goodness-of-fit of each model by defining a likelihood that compares the predicted and observed number of galaxies in each bin of r. In particular, we calculate each model's negative log-likelihood assuming that the errors are Poisson distributed.

$$-\ln L = \sum_{i \in r \text{ bin no.}} \ln(d_i!) + m_i - d_i \ln m_i \quad (7)$$

Here d_i is the number of galaxies in bin i and m_i is the number of galaxies in bin i predicted by the model. The set of parameters τ, α and ξ_{min} that produces the model that fits the data the best are the ones that minimises $-\ln L$ as this is equivalent to maximising the likelihood L (we call this maximum likelihood L_0). As $\ln(d_i!)$ becomes enormous and is constant across all the models anyway we set this term to zero and find the model that minimises this shifted log-likelihood, which will be the same as the one that minimises $-\ln L$, instead. We subtract this minimum shifted log-likelihood from all the shifted log-likelihoods to get the relative log-likelihood $\Delta \ln L = -\ln L - (-\ln L_0) = \ln L_0 - \ln L$. This is proportional to a likelihood ratio test, but we will stick to calling it relative log-likelihood and labeling this $\Delta \ln L$ as likelihood ratio tests are usually associated with the comparison of nested models. This is a more appropriate goodness-of-fit indicator than χ^2 in this case because several of the bins in the low-r tail have fewer than 5 galaxies and therefore have errors that are distributed significantly differently from a Gaussian and rebinning to ensure that all bins had at least 5 galaxies produced a binning that was too coarse.

5.1 Parameters

Slices from the $\Delta \ln L$ space are plotted in figure 6 for $\tau = [1.60, 1.99]$, $\alpha = [0.2000, 0.2195]$ and $\xi_{\text{min}} = [0.2500, 0.3865]$ with 40 equally spaced values in each range, i.e. $\Delta\tau = 0.01$ Gyr, $\Delta\alpha = 0.0005$ and $\Delta\xi_{\text{min}} = 0.0035$. The best-fitting model has $\tau = 1.79^{+0.046}_{-0.042}$ Gyr, $\alpha = 0.2095^{+0.0016}_{-0.0019}$ and $\xi_{\text{min}} = 0.3200^{+0.0149}_{-0.0135}$ and is plotted in figure 1. The given errors are statistical errors only, the errors owing to various assumptions and uncertainties in the model are much greater (see §6). As can be seen there are slight degeneracies between τ and ξ_{min} and between τ and α; if τ is increased a higher ξ_{min} and/or a lower α is preferred. This

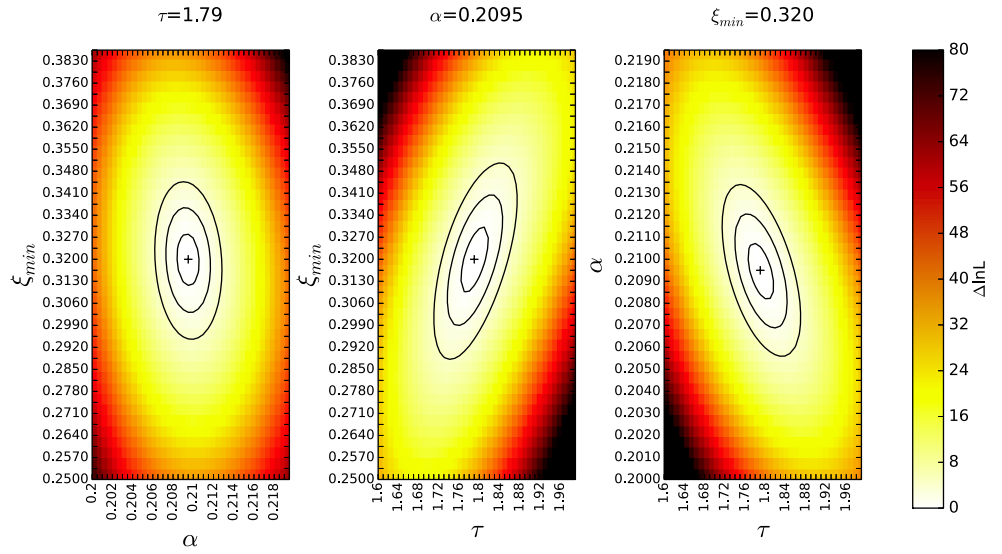

Figure 6. Contour plots of the $\Delta \ln L$ parameter space with one parameter set to its best-fitting value. The crosses mark the minimum while the black overplotted contours mark 1-σ, 2-σ and 3-σ deviations from the minimum (i.e. $\Delta \ln L = 0.5$, $\Delta \ln L = 2$ and $\Delta \ln L = 4.5$ respectively).

behaviour is quite intuitive: a higher number of galaxies showing diluted metallicities at a given time because the time-scale of metallicity depression is longer can be partially counteracted by excluding more merger mass ratios or making the effect of mergers on metallicity less severe.

The standard errors are found by marginalising the likelihood over the other two parameters for each parameter and finding the value of the parameter left and right of the peak where $L = e^{\frac{1}{2}} L_0$ (L_0 being the maximum likelihood) using linear interpolation between data points. This is done by numerically integrating the relative likelihood as found from $\Delta \ln L$ over the other two parameters. Using $\Delta \ln L$ rather than $-\ln L$ only changes the normalisation of the marginalised likelihood distribution. For example, in the case of α the marginalised likelihood distribution is given by

$$\begin{aligned} L(\alpha) &= \int_\tau \int_{\xi_{\min}} \exp(\Delta \ln L(\alpha, \tau, \xi_{\min}))\, \mathrm{d}\tau\, \mathrm{d}\xi_{\min} \\ &= \int_\tau \int_{\xi_{\min}} \exp(\ln L(\alpha, \tau, \xi_{\min}) - \ln L_0)\, \mathrm{d}\tau\, \mathrm{d}\xi_{\min} \\ &= \frac{1}{L_0} \int_\tau \int_{\xi_{\min}} L(\alpha, \tau, \xi_{\min})\, \mathrm{d}\tau\, \mathrm{d}\xi_{\min} \end{aligned} \quad (8)$$

$\frac{1}{L_0}$ can be found by requiring that the integral over all three parameters be unity.

The normalised parameter likelihood distributions are shown in figure 7. As can be seen, the distributions are approximately Gaussian and quite well resolved, meaning that the simple method used to derive the standard errors is appropriate, an assertion that is also supported by the fact that integrating from the left or right until 15.9 per cent of the area is enclosed yields nearly the same estimate of the errors.

To get a feel for how each of the parameters affects the model, we change one of the parameters by ± 50 per cent while keeping the other two parameters at their best-fitting value and the normalisation fixed. The resulting models are plotted in figure 8. As can be seen, increasing τ amplifies the tail while decreasing it brings the distribution closer to the best-fitting Gaussian. This is because increasing τ means that galaxies have diluted metallicities for a longer time and therefore the relative number of galaxies showing depressed metallicity at any one point in time increases. Varying α changes the overall shape of the tail with larger values causing a decrease of the moderate low-r part and an increase of the more extreme offsets and smaller values bringing the distribution closer to a Gaussian that is wider than the best-fitting one. This is because increasing α increases the magnitude of metallicity dilution moving galaxies that are already experiencing dilution further towards lower metallicities. Increasing/decreasing $\xi_{\min}$ diminishes/amplifies the moderate part of the tail while having no influence at the more extreme offsets. This is because increasing $\xi_{\min}$ removes the galaxies at the lowest mass ratios previously included which therefore have the smallest metallicity dilutions.

6 DISCUSSION

6.1 Magnitude and time-scale of the metallicity dilution

The magnitude of the nuclear metallicity dilution caused by a merger is connected to the parameter α in our model. Because star formation is enhanced during a merger and the FMR is inversely correlated with SFR the change in r in our model is a lower limit on the change in nuclear metallicity during a merger. In practice, however, both the SFR dependence of our fitted FMR and the increase in SFR in the tail relative to the general population are small enough that we can safely ignore this (the difference in median SFR between the general population and the tail by itself only leads to $\Delta r = -0.003$). The same is true for mass (the difference in mass leads to $\Delta r = -0.02$) so we can equate the change in r with the change in nuclear metallicity without introducing any significant uncertainty.

The best-fitting value of $\alpha = 0.2095$ implies that the nuclear metallicity will on average decrease by about 0.2 dex during a 1:1 merger in agreement with the simulations of Montuori et al. (2010) and Rupke et al. (2010) who found metallicity depressions to be in

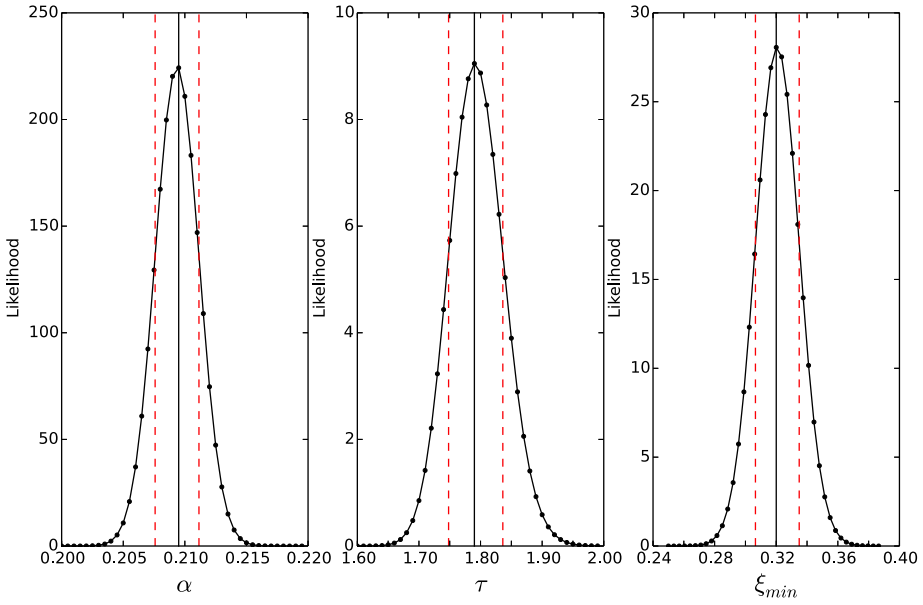

Figure 7. Marginalised parameter space for α, τ and $\xi_{\rm min}$ from left to right. The unbroken line marks the parameter value that yields the maximum likelihood L_0 (with no interpolation between the parameter values used in the simulation). Dashed lines mark the formal standard errors as estimated by the linearly interpolated parameter values left and right of L_0 that lead to $L = e^{1/2}L_0$.

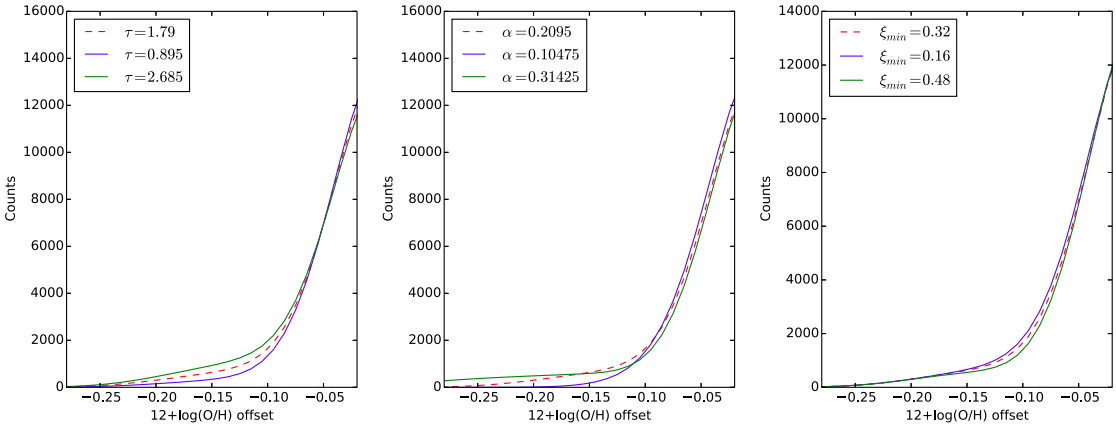

Figure 8. The best-fitting model (dashed, red line) has one of its parameters decreased by 50 per cent (blue line) and increased by 50 per cent (green line) while the two other parameters and the normalisation are held fixed. From left to right τ, α and $\xi_{\rm min}$ are varied.

the range 0.2 dex – 0.3 dex and 0.1 dex – 0.3 dex, respectively. Both of these were smoothed-particle hydrodynamics simulations of equal mass mergers with Montuori et al. (2010) being the more sophisticated of the two by including star formation and chemical enrichment from supernovae.

We calculate the average metallicity decrease for all mass ratio mergers included in a given model as $\int_{-0.5}^{0.5} rP(r|\mathrm{merged})P(\mathrm{merged})c_{\rm norm}\,\mathrm{d}r$ where $c_{\rm norm} \equiv \left(\int_{-0.5}^{0.5} P(r|\mathrm{merged})P(\mathrm{merged})\,\mathrm{d}r\right)^{-1}$ (see §4 for the definitions of $P(r|\mathrm{merged})$ and $P(\mathrm{merged})$) and find that this is 0.116 dex for our best-fitting model. This is a somewhat more modest decrease than the 0.17 dex metallicity difference we find in the median metallicities between our general sample (which is very close to the difference between the averages) and the galaxies in the tail. However, this value is quite sensitive to the definition of where the tail begins, which we chose to be 2σ below the mean r to be able to clearly distinguish the population in the tail from the general population. If, for example, the tail is defined to begin at 1.5σ below the mean r instead, the galaxies in the tail have an average metallicity deficiency of 0.13 dex.

Comparing our average metallicity dilution of 0.116 dex to observations of close galaxy pairs in the SDSS, Kewley et al. (2006) found that pairs with separations < 20 kpc followed a luminosity-metallicity (LZ) relation that was systematically shifted relative to the LZ relation for field galaxies by -0.2 dex but Ellison et al.

(2008b) argued that roughly half of this shift is due to luminosity so correcting for this puts their observed metallicity dilutions close to our value. However, studies by Ellison et al. (2008b), Scudder et al. (2012) and Michel-Dansac et al. (2008) find a smaller change of -0.03 to -0.05 dex. Most of this discrepancy is due to the use of different lower mass ratio limits. Ellison et al. (2008b) and Scudder et al. (2012) both included mergers down to a mass ratio of 1:10 while our best-fitting model has $\xi_{\rm min} = 0.32$, i.e. only includes mergers down to a mass ratio of about 1:3. Keeping the other parameters at their best-fitting value but setting $\xi_{\rm min} = 0.1$ yields an average metallicity depression of 0.073 dex. Michel-Dansac et al. (2008) does not employ a sharp mass ratio cutoff but they do plot the mass-metallicity relation (MZR) for all galaxies versus interacting galaxies for $\xi_* < 0.2$ and $\xi_* > 0.2$ with the larger interactions showing much stronger dilution (see their figure 2).

The parameter τ should be the average time from the moment when the metallicity becomes diluted due to a merger until it completely recovers. Unfortunately most numerical simulations of merger-induced metallicity dilution are not run sufficiently long to estimate this time-scale and as such only yield lower limits. However we find our best-fitting value of 1.79 Gyr to be in good agreement with the typical metallicity depression time of ~ 2 Gyr found in Montuori et al. (2010) and above the lower limit of 1 Gyr found in Torrey et al. (2012).

In our model the metallicity depression is constant in time and lasts the same for all mergers. However simulations show that for any particular merger both the magnitude and length of metallicity depression depends in complicated ways on the orientations of the galaxies and on wether they are on retrograde or prograde orbits. The metallicity depression time-scale probably also depends on mass ratio (see §6.5). Furthermore Torrey et al. (2012) found that the initial gas fractions of the galaxies are important with higher gas fractions leading to less dilution. A characteristic feature found to some degree in all merger simulations is a "double-dip" shape of the metallicity as function of time associated with the first and second pericentric passages. We chose to ignore these complications as their effects are not well known and including any of them would add significant complexity to our model ruining its appealing simplicity. Furthermore, because we are using a rather large sample, our model should still yield representative average values of the dilution magnitude and time-scale.

6.2 Merger rate

Galaxy-galaxy merger rates have significant uncertainties pertaining to the halo-halo merger rate, the stellar mass-halo mass relation used to convert halo masses to stellar masses and the method used to follow sub-haloes or the assumed merger delay, either of which are used to convert the halo-halo merger rate to a galaxy-galaxy merger rate (see Hopkins et al. 2010b for a detailed analysis of each source of uncertainty in merger rates). For a halo-halo merger rate derived from a simulation such as the one we use from Fakhouri et al. (2010) (which is based on the Millennium and Millennium-II simulations) there are uncertainties from the definition of mass ratios, the construction of merger trees and the time resolution in the simulation. These yield a combined uncertainty of factor ~ 2.

A source of uncertainty that we introduce in converting this to a galaxy-galaxy merger rate is that we do not include any merger delay, i.e. we assume that the time that passes from one of the haloes to become a subhalo to the merger is completed is the same for all galaxies. This merger delay is often calculated based on a model of inspiral due to dynamical friction in which case it depends on mass ratio, virial radius of the primary galaxy and the energy and angular momentum of the orbit (see e.g. Jiang et al. (2008) or Boylan-Kolchin et al. (2008)). Other methods based on characteristic time-scales for gravitational or angular momentum capture can also be used (see Hopkins et al. (2010a)). In general ignoring the merger delay time yields fewer major mergers. The differences in merger rates arising from using different merger delays or subhalo-following methods was examined in Hopkins et al. (2010b) and Hopkins et al. (2010a) where it was found that the merger rate derived using no delay or method to follow subhaloes lay within the range of merger rates derived using these methods. More importantly we are interested in galaxies with diluted metallicities due to mergers which may well be a process that scales differently with various parameters and begins and ends at different times than the merger itself as measured from some dynamical friction or group capture time-scale.

At low stellar masses of $\log(M_*/M_\odot) \lesssim 10$ the gas fraction is significantly greater than at high stellar masses so our using the stellar mass ratio ξ_* underestimates the actual metallicity impact, which should depend on the total tightly bound mass, of low-M_* mergers by a factor of at least ~ 3 (Hopkins et al. 2010b).

A consequence of defining mass ratio as $\xi_* = \frac{M_{*,\rm secondary}}{M_{*,\rm primary}} \leqslant 1$ is that we are ignoring the secondary members of mergers in our model. The degree of uncertainty caused by this depends on two factors: the number of such galaxies in our sample and how the metallicity of smaller companions in a merger changes. For a given stellar mass we can estimate the fraction of mergers as the primary galaxy from the merger rate and the galaxy stellar mass function. Based on this calculation and the stellar mass distribution of the galaxies in our sample we roughly estimate that if the secondary galaxy was affected similarly to the primary galaxy τ would be overestimated by a factor of ~ 4 in our model. This calculation is detailed in appendix A.

The effect on the metallicity of a galaxy caused by it merging with a more massive galaxy has not been examined in any detail but we would expect *enrichment* rather than dilution in this case as the smaller galaxy accretes more enriched gas from the larger galaxy which also triggers star formation. Indeed Scudder et al. (2012) found that both members of merging pairs experienced similar levels of SFR enhancement and Michel-Dansac et al. (2008) found that while massive galaxies in mergers showed diluted metallicities smaller merging galaxies with $\log(M_*)/M_\odot \lesssim 10$ showed enrichment instead. Therefore we expect the vast majority of galaxies that are merging or have recently merged as a secondary member to not be in the low-r tail and the effect on our results of ignoring these should be small.

We can roughly estimate the merger fraction of our sample assuming that all galaxies in excess of the best-fitting Gaussian for the FMR residuals below the mean are merging. We find a merger fraction of 5.25 per cent of the sample in this way. As we are ignoring flybys (see §6.3) and metallicities recover on a time-scale that is longer than the time-scale of the merger being visible (as either clear morphological disturbances or galaxy pairs) this is an upper limit. We cannot compare this directly to observational measurements of the merger fraction as these are measured for high masses (typically $M_* > 10^{10} M_\odot$) or luminosities only and for different types of samples (as we filtered out AGNs and galaxies without active star formation) at typically significantly higher redshifts. However our value lies within the range of results in the literature found

from morphological merger indicators (generally 1–10 per cent at lower redshifts; see Lotz et al. (2011)).

6.3 Flybys

A potentially important complication that we are ignoring is flybys i.e. when a galaxy passes another galaxy at a small distance but does not merge. We chose not to include flybys as the current quantitative knowledge of the effect and rate of flybys is poor and because of the considerable complexity it would add to our model. Little work has been done to examine the effects of flybys on metallicity. However Montuori et al. (2010) found that in their simulations of equal-mass interactions close flybys caused almost as much nuclear metallicity dilution as mergers and that this dilution lasted for almost as long as for mergers.

The flyby rate has also received very little study. Sinha & Holley-Bockelmann (2012) found from cosmological N-body simulations that the rate of "grazing" flybys (i.e. when two primary haloes approach each other, overlap for at least half a crossing time, then continue on different trajectories as two distinct primary haloes again) was comparable to the merger rate for halo masses $\log(M_h/M_\odot) \gtrsim 11$ (corresponding to $\log(M_*/M_\odot) \gtrsim 9$) at $z \lesssim 2$.

In the simple scenario where the flyby rate is equal to the merger rate and flybys dilute the nuclear metallicity in a way similar to mergers and on the same time-scale, the full effect of ignoring flybys in our model is simply that τ will be overestimated by a factor of 2. While this simple situation might not be that far from the truth considering the findings of Montuori et al. (2010) and Sinha & Holley-Bockelmann (2012) we expect the magnitude of dilution to depend on the pericentric distance of the flyby with greater distances causing less dilution.

6.4 Metallicity calibrations

As different metallicity calibrations yield quite different metallicities and mass-metallicity relations (see Kewley & Ellison (2008)) we expect the choice of calibration to have an impact on the FMR. To evaluate the impact of different calibrations we compare the shape of the distribution of residuals of the fitted FMR and nature of the low-r tail of the data based on the N2 calibration of Denicoló et al. (2002), the R23 calibration of Maiolino et al. (2008) and the average of these two which was used in M10 with the previous data based on the O3N2 calibration of Marino et al. (2013). We show the FMR residual distributions for these calibrations in figure 9.

As with O3N2 these calibrations have limited ranges of validity, though both are broad. N2 has a range of $7.2 < 12 + \log(\mathrm{O/H}) < 9.1$ and the entire sample lies within this. The range for R23 is about $7.0 < 12 + \log(\mathrm{O/H}) < 9.3$ and 99 per cent of the sample lies within this range.

Denicoló et al. (2002) finds a relation for $12 + \log(\mathrm{O/H})$ as a linear function of $\mathrm{N2} = [\mathrm{NII}]\lambda6584/\mathrm{H}\alpha$. Using this relation to find the metallicities and fitting an FMR to these we find that the metallicity dispersion is not too dissimilar to the dispersion based on O3N2. Fitting a Gaussian distribution with least squares as before we find an almost identical scatter of $\sigma = 0.044$ dex and a slightly lower mean of $\mu = 0.002$ dex. The tail is smaller though, containing an excess of about 2.3 per cent of all galaxies. There is a systematic offset towards lower metallicities of 0.05 dex for the entire population and the tail alike. The SSFRs of the galaxies in the tail have a median value that is 0.12 dex higher than for O3N2 (i.e. 0.42 dex higher than the median SSFR of the general population). This is due to there being about the same number of galaxies with $\log(SSFR) > -10$ as there are for O3N2 while there are fewer galaxies with lower SSFRs rather than the overall distribution being shifted.

Maiolino et al. (2008) find a relation of $12 + \log(\mathrm{O/H})$ as a polynomial function of $\mathrm{R23} = ([\mathrm{OII}]\lambda3727 + [\mathrm{OIII}]\lambda4959 + [\mathrm{OIII}]\lambda5007)/\mathrm{H}\beta$. In this case we find a much wider and more skewed metallicity dispersion distribution with a scatter of $\sigma = 0.078$ dex and mean $\mu = 0.011$ dex. The tail is bigger containing an excess of about 5.3 per cent of all galaxies. As with N2 there is a systematic offset in the metallicities of 0.05 dex but towards higher rather than lower metallicities. The median SSFR of the galaxies in the tail are lower than for O3N2 by 0.12 dex (i.e. 0.18 dex higher than the median SSFR of the general population). As in the case of N2 this is due to the low-SSFR part with $\log(SSFR) < -11$ being enhanced relative to the high-SSFR part rather than an overall offset.

Finally we look at the average of the N2 and R23 metallicities as was used in M10. In this case the scatter is slightly smaller at $\sigma = 0.044$ dex while the mean is slightly larger at $\mu = 0.0088$ dex. However while the scatter is small the tail is large with an excess of 6.9 per cent of all galaxies. There is a systematic offset towards higher metallicities of 0.26 dex. The SSFRs in the tail have a median value that is 0.07 dex lower than for O3N2 (i.e. 0.23 dex higher than the general population). M10 used the N2 calibration of Maiolino et al. (2008) but we use the Denicoló et al. (2002) calibration because a sizeable fraction of the galaxies in our sample have $\log([\mathrm{NII}]\lambda6564/\mathrm{OII}\lambda3727) < 1.2$ for which the Maiolino et al. (2008) calibration is not valid. However, for the subset of galaxies that do have valid Maiolino et al. (2008) N2 metallicities the residual distribution is quite similar to the Maiolino et al. (2008) R23 metallicities.

From these comparisons it is clear that while the shape of the metallicity dispersion around the FMR changes with the calibration used, a low-r tail containing galaxies with generally lower metallicities and higher SSFRs than the general population is present across at least the three popular metallicity calibrations based on O3N2, N2 and R23. Thus our qualitative conclusion that the tail is consistent with reflecting the impact of mergers is unchanged and the uncertainties in the inferred model parameters arising from different metallicity calibrations seem to be no greater than the uncertainties caused by e.g. uncertainties in the merger rate or ignoring flybys.

6.5 Aperture effects

As we use a 3 arcsec aperture for measuring SFRs and metallicities these quantities represent only the central 4–11 kpc of the galaxies in our redshift range. This leads to systematic changes with redshift (in addition to any effects from cosmic evolution) as the fiber on average covers larger parts of galaxies at higher redshifts. There is a slight difference in the median redshifts of the low-r tail ($z = 0.117$) and the general population ($z = 0.107$) but this only leads to an 8 per cent difference in median angular sizes. In order to assess the magnitude of aperture effects we split our full sample into two equally sized subsamples: a low-redshift sample containing galaxies with redshift below the overall median redshift of our sample and a high-redshift sample containing galaxies with redshift above the median redshift. We then fit our model to these two subsamples in the same way as for the full sample, i.e. we fit an FMR and a Gaussian to the distribution of metallicity residuals

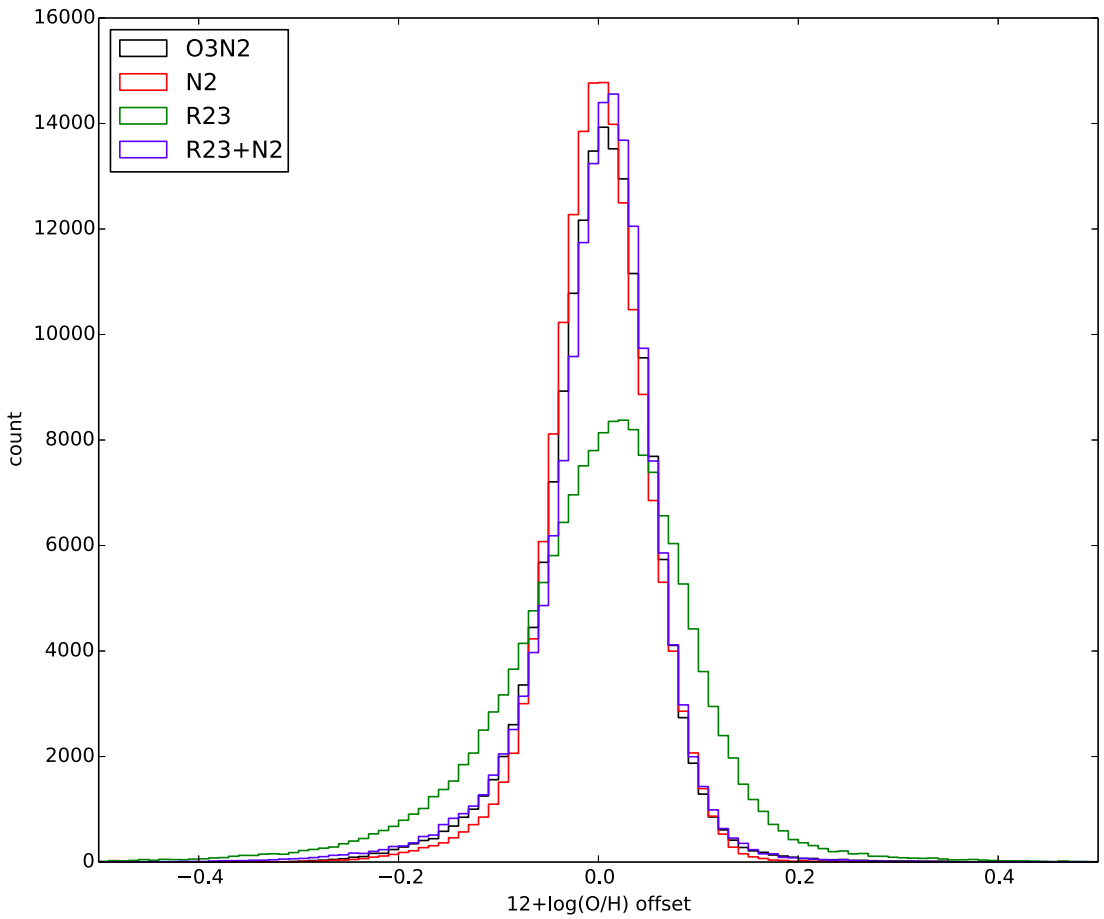

Figure 9. The FMR residuals of different metallicity calibrations. The black line is the residuals of the O3N2 calibration of Marino et al. (2013) that we have been using while the red, green and blue lines are residuals of calibrations based on N2 (Denicoló et al. 2002), R23 (Maiolino et al. 2008) and the average of those two, respectively.

and fit another Gaussian only within two standard deviations from the mean found from the first fit to avoid the tails and then input the standard deviation and mean found to our merger model.

We find that the best-fitting value of α is very similar for the high-redshift sample and full sample while it is a bit lower for the low-redshift sample ($\alpha = 0.205$, 0.210 and 0.2095 for the low-redshift, high-redshift and full samples, respectively). While the low-redshift value is more than two sigma below the full sample value it only leads to physically insignificant changes in metallicity dilution magnitudes. The best-fitting value of τ is 0.50 Gyr higher for the low-redshift sample and 0.25 Gyr lower for the high-redshift sample compared to the best-fitting τ for the full sample of 1.79 Gyr. The best-fitting $\xi_{\rm min}$ is slightly smaller by 0.054 for the low-redshift sample and slightly larger by 0.036 for the high-redshift sample compared to the best-fitting value of 0.32 for the full sample. The fitted Gaussian that excludes the tails has a slightly smaller scatter for the low-redshift sample ($\sigma = 0.045$ dex) than the full sample which has $\sigma = 0.047$ dex while the high-redshift sample has approximately the same scatter. As $\xi_{\rm min}$ represents the smallest merger that produces a metallicity change that can be differentiated from the intrinsic scatter in the FMR we would expect it to increase/decrease if the scatter increases/decreases. As such the difference in $\xi_{\rm min}$ across the samples is as expected seeing how both $\xi_{\rm min}$ and the scatter is smaller for the low-redshift sample while $\xi_{\rm min}$ is only slightly greater and the scatter is the same for the high-redshift sample compared to the full sample.

The decrease in τ with redshift might be mainly due to the increase of $\xi_{\rm min}$ with redshift. The merger time decreases with mass ratio (Hopkins et al. 2010a), if the metallicity depression time-scale has this trend as well the lower $\xi_{\rm min}$ found at lower redshifts will cause the model to have a larger contribution from smaller mass ratio mergers with longer time-scales which will drive the average time-scale τ up. Furthermore the merger time also depends on the virial time $t_{\rm vir} = \frac{R_{\rm vir}}{v_{\rm vir}}$ which evolves with redshift as $t_{\rm vir} \propto (1+z)^{3/2}$ but this only causes a 7 per cent increase in $t_{\rm vir}$ from the median redshift of the low-redshift sample $z = 0.085$ to the median redshift of the high-redshift sample $z = 0.138$ and the virial time is only one part of the merger time which again is only one part of the dilution time. That τ and $\xi_{\rm min}$ change with redshift in a way that is different from the degeneracy between the two (see §5.1) indicates that this effect is not due to random errors.

Overall the differences in the best-fitting model parameters between the low-redshift and the high-redshift subsamples are fairly small and can be explained by effects other than aperture effects.

7 CONCLUSIONS

Fitting an FMR to our large sample of SDSS galaxies we have shown that the tail in the distribution of the FMR residuals towards lower metallicities forms a distinct population and that many of these might be merging or have recently merged given their enhanced SSFRs. Our simple model is able to successfully reproduce the observed distribution of FMR residuals yielding metallicity depressions and dilution time-scales that are in good agreement with the results of merger simulations and observations of galaxy pairs.

We find that the average metallicity depression caused by a 1:1 merger is about 0.2 dex in agreement with the hydrodynamical simulations of Montuori et al. (2010) and Rupke et al. (2010). We also find the average depression of all major mergers ($\xi_* > 0.32$) to be 0.116 dex which is consistent with the actual metallicity difference of the tail compared to the entire sample. This is a greater dilution than what is found in the metallicity measurements of SDSS pair samples of Ellison et al. (2008b), Scudder et al. (2012) and Michel-Dansac et al. (2008) but our value is consistent with those studies when the differences between the minimum mass ratios in those samples and in our model are taken into account.

We find that the average metallicity depression time-scale (the time from the onset of metallicity dilution until recovery to the pre-merger value) due to a merger is 1.79 Gyr in good agreement with the merger simulations of Montuori et al. (2010).

Currently the quantitative knowledge of the rate and effect of galaxy flybys is very poor. However in the future as our understanding of flybys increases, the precision of our model can be significantly increased by extending the formalism to include flybys in addition to mergers. In addition, future hydrodynamical merger simulations more comprehensive than the merger simulations done so far, that probe the entire range of galaxy masses and mass ratios could allow for a more specific estimation of the dilution time-scale. Provided such a simulation is run for a sufficiently long time so that any potential stellar mass and mass ratio dependence of the metallicity depression time-scale can be found it would allow our model to predict this time-scale for mergers of different member masses rather than as averaged over all mergers. In addition such a simulation might probe whether the mass ratio dependence of the metallicity depression (as time-averaged between pericentric passages) is approximately linear as we assume or has a more complicated form.

Our model makes some predictions that might be tested observationally. Low-metallicity outliers from the FMR should have a higher pair fraction than the general population and the mass ratios of pairs should be closer to unity as one moves to greater metallicity depressions. For theorists large-scale hydrodynamical simulations that track the metallicity of thousands of galaxies such as Illustris (Vogelsberger et al. 2014; Genel et al. 2014) should enable a statistical study of merger induced metallicity dilution that could test whether the galaxies in the low-metallicity tail are really interacting (or have recently interacted) and in that case compare their inferred dilution time-scale, magnitude of metallicity depression and mass ratio dependence of those with our results.

ACKNOWLEDGMENTS

The Dark Cosmology Centre is funded by the DNRF. We thank Sara Ellison and Filippo Mannucci for helpful discussions.

Funding for SDSS-III has been provided by the Alfred P. Sloan Foundation, the Participating Institutions, the National Science Foundation, and the U.S. Department of Energy Office of Science. The SDSS-III web site is http://www.sdss3.org/.

SDSS-III is managed by the Astrophysical Research Consortium for the Participating Institutions of the SDSS-III Collaboration including the University of Arizona, the Brazilian Participation Group, Brookhaven National Laboratory, Carnegie Mellon University, University of Florida, the French Participation Group, the German Participation Group, Harvard University, the Instituto de Astrofisica de Canarias, the Michigan State/Notre Dame/JINA Participation Group, Johns Hopkins University, Lawrence Berkeley National Laboratory, Max Planck Institute for Astrophysics, Max Planck Institute for Extraterrestrial Physics, New Mexico State University, New York University, Ohio State University, Pennsylvania State University, University of Portsmouth, Princeton University, the Spanish Participation Group, University of Tokyo, University of Utah, Vanderbilt University, University of Virginia, University of Washington, and Yale University.

REFERENCES

Andrews, B. H., & Martini, P. 2013, ApJ, 765, 140
Baldry, I. K., et al. 2012, MNRAS, 421, 621
Behroozi, P. S., Conroy, C., & Wechsler, R. H. 2010, ApJ, 717, 379
Boylan-Kolchin, M., Ma, C.-P., & Quataert, E. 2008, MNRAS, 383, 93
Chabrier, G. 2003, PASP, 115, 763
Cooper, M. C., Tremonti, C. A., Newman, J. A., & Zabludoff, A. I. 2008, MNRAS, 390, 245
Denicoló, G., Terlevich, R., & Terlevich, E. 2002, MNRAS, 330, 69
Ellison, S. L., Patton, D. R., Simard, L., & McConnachie, A. W. 2008a, ApJ, 672, L107
Ellison, S. L., Patton, D. R., Simard, L., & McConnachie, A. W. 2008b, AJ, 135, 1877
Erb, D. K., Shapley, A. E., Pettini, M., Steidel, C. C., Reddy, N. A., & Adelberger, K. L. 2006, ApJ, 644, 813
Fakhouri, O., Ma, C.-P., & Boylan-Kolchin, M. 2010, MNRAS, 406, 2267
Genel, S., et al. 2014, ArXiv e-prints, 1405.3749
Henry, A., et al. 2013, ApJ, 776, L27
Hopkins, P. F., et al. 2010a, ApJ, 715, 202
Hopkins, P. F., et al. 2010b, ApJ, 724, 915
Jiang, C. Y., Jing, Y. P., Faltenbacher, A., Lin, W. P., & Li, C. 2008, ApJ, 675, 1095
Kauffmann, G., et al. 2003, MNRAS, 341, 33
Kennicutt, R. C., Jr. 1998, ARA&A, 36, 189
Kewley, L. J., & Ellison, S. L. 2008, ApJ, 681, 1183
Kewley, L. J., Geller, M. J., & Barton, E. J. 2006, AJ, 131, 2004
Lara-López, M. A., et al. 2010, A&A, 521, L53
Lequeux, J., Peimbert, M., Rayo, J. F., Serrano, A., & Torres-Peimbert, S. 1979, A&A, 80, 155
Lotz, J. M., Jonsson, P., Cox, T. J., Croton, D., Primack, J. R., Somerville, R. S., & Stewart, K. 2011, ApJ, 742, 103
Luck, R. E., & Lambert, D. L. 2011, AJ, 142, 136
Maiolino, R., et al. 2008, A&A, 488, 463
Mannucci, F., Cresci, G., Maiolino, R., Marconi, A., & Gnerucci, A. 2010, MNRAS, 408, 2115
Mannucci, F., Salvaterra, R., & Campisi, M. A. 2011, MNRAS, 414, 1263
Marino, R. A., et al. 2013, A&A, 559, A114

Michel-Dansac, L., Lambas, D. G., Alonso, M. S., & Tissera, P. 2008, MNRAS, 386, L82
Mihos, J. C., & Hernquist, L. 1996, ApJ, 464, 641
Montuori, M., Di Matteo, P., Lehnert, M. D., Combes, F., & Semelin, B. 2010, A&A, 518, A56
Peeples, M. S., Pogge, R. W., & Stanek, W. Z. 2009, ApJ, 695, 259
Perez, J., Michel-Dansac, L., & Tissera, P. B. 2011, MNRAS, 417, 580
Pettini, M., & Pagel, B. E. J. 2004, MNRAS, 348, L59
Rupke, D. S. N., Kewley, L. J., & Barnes, J. E. 2010, ApJ, 710, L156
Scudder, J. M., Ellison, S. L., Torrey, P., Patton, D. R., & Mendel, J. T. 2012, MNRAS, 426, 549
Sinha, M., & Holley-Bockelmann, K. 2012, ApJ, 751, 17
Torrey, P., Cox, T. J., Kewley, L., & Hernquist, L. 2012, ApJ, 746, 108
Tremonti, C. A., et al. 2004, ApJ, 613, 898
Vogelsberger, M., et al. 2014, ArXiv e-prints, 1405.2921
Zaritsky, D., Kennicutt, R. C., Jr., & Huchra, J. P. 1994, ApJ, 420, 87

APPENDIX A: ESTIMATING THE POTENTIAL IMPACT OF SECONDARY MERGER MEMBERS

Given the merger rate per galaxy per stellar mass ratio per lookback time $\frac{\mathrm{d}^2 P}{\mathrm{d}\,\xi_*\,\mathrm{d}\,t}(M_*, \xi_*, t)$ for *primary* merger members, i.e. $\xi_* \leqslant 1$, and the distribution of galaxy stellar masses $\phi(M_*)$ (defined such that $\phi(M)\,\mathrm{d}M$ is the number of galaxies per volume with stellar mass between M and $M + \mathrm{d}M$) we can calculate the rate of mergers per galaxy that galaxies of a given mass experience as the *secondary* member, i.e. $\xi_* > 1$.

$$\frac{\text{mergers}}{\text{time} \cdot \text{galaxy}}(\xi_* > 1, M_0) = \frac{\int_{M_0+\delta M}^{\infty} \phi(M_{\text{pri}}) \int_{(M_0+\delta M)/M_{\text{pri}}}^{M_0/M_{\text{pri}}} \frac{\mathrm{d}^2 P}{\mathrm{d}\,\xi_*\,\mathrm{d}\,t}\,\mathrm{d}\xi_*\,\mathrm{d}M_{\text{pri}}}{\int_{M_0}^{M_0+\delta M} \phi(M)\,\mathrm{d}M} \quad \text{(A1)}$$

where the merger rate is evaluated at M_{pri}, ξ_*, and $t = 1.30$ Gyr which corresponds to $z = 0.1$, the typical redshift of our sample. We use the mass function of Baldry et al. (2012). If we assume that the metallicity of these galaxies is affected in the same way as the primary galaxies we can get a rough estimate of the overall error θ that ignoring secondary galaxies introduces in the dilution timescale τ. We define

$$R_{\text{pri}}(M) \equiv \frac{\text{mergers}}{\text{time} \cdot \text{galaxy}}(\xi_{\text{min}} < \xi_* < 1, M)$$

and

$$R_{\text{sec}}(M) \equiv \frac{\text{mergers}}{\text{time} \cdot \text{galaxy}}(\xi_* > 1, M)$$

and calculate θ by integrating the fraction of merging galaxies that are primary at each mass over the mass distribution of our sample.

$$\theta = \frac{\tau_{\text{corrected}}}{\tau} = \frac{\int_0^{\infty} \frac{\mathrm{d}\,P}{\mathrm{d}\,M} \frac{R_{\text{pri}}}{R_{\text{pri}}+R_{\text{sec}}}\,\mathrm{d}M}{\int_0^{\infty} \frac{\mathrm{d}\,P}{\mathrm{d}\,M}\,\mathrm{d}M} \quad \text{(A2)}$$

For the best-fitting value of $\xi_{\text{min}} = 0.32$ we find $\theta = 0.27$ so τ would be overestimated by a factor ~ 4.